Mathematical Biology — *Modeling blood filtration in hollow fibers dialyzers coupled with patient's body dynamics*, by CLAUDIO RONCO, FRANCESCO GARZOTTO, JEONG CHUL KIM, ANTONIO FASANO, IACOPO BORSI and ANGIOLO FARINA, communicated on 11 December 2015.

ABSTRACT. — We develop a mathematical model for cross filtration in a hollow fibers dialyzer, taking into account not only the phenomena occurring within the machine, but also the redistribution of chemicals between intra- and extracellular compartments in the patient's body. The scheme for the cross flow is derived with reference to a single fiber, starting from the basic laws of fluid dynamics and exploiting the smallness of the ratio between the fiber radius and the fiber length to obtain significant simplifications. We end up with a system of integral and partial differential equations in which the input data are in principle unknown. Indeed, the blood composition is considerably altered while going through the fiber and the body reacts redistributing urea, sodium ions, etc. between intra- and extracellular compartments with its own dynamics, thus updating the various concentrations at the dialyzer inlet. Such a coupling is an essential feature of the model. We present numerical simulations, showing a reasonable agreement with the data for a specific patient taken from the literature.

1. INTRODUCTION

Hollow-fiber dialyzers perform blood purification very efficiently and are widely used in the medical practice. They consist of a bundle of porous fibers with a channel through which blood is forced by a driving pressure gradient. The diameter of pores is in the range of a few tens of nanometers, the one needed for cross-filtration processes, allowing the passage of water and light solutes, but not of large molecules such as albumin (MW 66.5 kDa) and red blood cells. Thus the fibers behave to plasma as semipermeable membranes and such a property is associated with the onset of osmosis, a phenomenon in continuous evolution due to the progressive water migration through the membranes. In the complementary space of the device a fluid (dialyzate) flows, carrying away the filtrate. The dialyzate is given an appropriate composition so to match the physiological concentrations of electrolytes and solutes, thus preventing their loss during the process. The literature on hemodialysis by ultrafiltration is very large (we refer the reader to [40], [44] and the literature therein) and includes several papers on mathematical modeling. Models are generally of compartmental type (see e.g. [57]), based on ordinary differential equations, with some notable exception.

In particular [2], considers flows through a hollow fiber with a spatial structure, in the same spirit of the present work.

Here we want to formulate a new mathematical model for the three flows in the dialyzer (blood flow, dialyzate flow, cross flow), based on the method of upscaling, which exploits the smallness of the ratio ε between the radius of the fibers and its length (order 10^{-4}). The fundamental advantage of this method (upscaling) is the fact that it stems from the basic laws of fluid dynamics and, expanding of all the quantities involved in powers of ε and matching terms with equal powers in the governing equations, leads to approximating equations at the desired order in ε. Actually, the approximation to the order ε^0 is all we need. It will be derived in Section 4, after having introduced the basic equations (Sect. 2) and their appropriate dimensionless version (Sect. 3), based on a double scaling of spatial and kinetic coordinates (in the longitudinal and in the radial directions).

A basic feature emphasized by the model above is the fact that the inlet values of the main quantities (hematocrit, proteins concentration, electrolytes concentrations) are not known. Indeed the composition of the blood which is returned to the patient has undergone a dramatic change in the device. It is of fundamental importance to determine the hematological parameters of the blood returning to the machine, which are the result of a dynamics taking place in the patient's body, tending to redistribute water, urea, sodium, etc. among various compartments (cells, interstices, blood). Therefore the mathematical model for the dialyzer has to be complemented by another model expressing the kinetics of compartmental redistribution of the relevant quantities. Such a task is carried out in Sect. 5, along with a discussion of the delicate issue of selecting the initial conditions. Our approach tries to avoid as much as possible heuristic approximations and to preserve the physical complexity of the process, though making use of all the powerful simplifications engendered by the upscaling method. In this it differs substantially from other similar papers like [2], [57], [3] and others.

In Sect. 6 we introduce a simplification by choosing a rheological model of blood in which we ignore shear thinning, but just allow viscosity to depend on hematocrit and on proteins concentration. Eventually, we perform some numerical simulation. A crucial step (irrespective of the blood rheological model) is to realize that the dialyzer on one side and the body on the other have dynamic responses exhibiting very different time scales (10 seconds and 10^3 seconds, respectively). The consequence is that the evolution of the inlet values in the dialyzer is definitely slow in its own time scale, so that all quantities evolve in a quasi-stationary way, leading to a very substantial simplification of the numerical procedure. The results show that the model is capable of effectively describing a hemodialysis session, though for simplicity phenomena like membrane fouling and albumin deposition are neglected. We plan to incorporate them in a future paper.

2. Definitions and basic assumptions

A dialyzer module consists of an array of a large number of parallel hollow fibers. By symmetry, except for small disturbances, all fibres are surrounded by
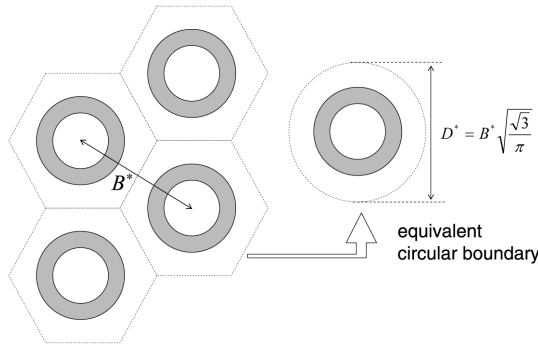
Figure 1. The bee nest no-flux interfaces and the equivalent geometry.

a "virtual" no-flux boundary, confining the permeate flow, with the exception of the peripheral fibres (a small fraction of the total number).

We assume that the set of no-flux boundaries has a bee-nest structure (Fig. 1). We replace the original hexagonal cell by an equivalent circular cylinder whose external radius[1] D^* is chosen as a function of the mutual distance between the axes of adjacent fibres, B^*. According to the criterion of preserving the cross section, discussed in [5], we set[2] $(D^*/B^*)^2 = \sqrt{3}/\pi$ (see again Fig. 1). Hence, we consider the fiber bundle as an array of identical hollow cylinders surrounded by a "virtual" cylindrical no-flux boundary.

We now focus on a single cell, Fig. 2, with the caveat that inlet and outlet pressures applied to the bundle as a whole may not be uniformly distributed[3] [29], [41], [42]. The idea of working with single axisymmetric element is alternative to the approach of averaging all relevant quantities over representative elementary volumes in the spirit of continuum mechanics (see [44] and the literature quoted therein). We denote by R^*, and H^*, the internal and external radius of the fiber, respectively. The fiber thickness is $S^* = H^* - R^*$, and the length is L^* (see Fig. 2).

Typically, introducing the aspect ratio

$$\varepsilon = \frac{R^*}{L^*},$$

we have $\varepsilon \ll 1$.

Owing to the symmetry, we consider only a longitudinal and a radial coordinate (x^*, r^*). The domain can be divided into three regions (see Fig. 3):

---

[1] Throughout this paper the superscript "*" denotes dimensional variables.

[2] Indeed, the area of the set of the points which are not in the intersection of the hexagon and of the circle is about 1% of the area of each of the two domains. We expect the perturbation on the main quantities to be of the same order.

[3] Generally averaging pressure in the two flows in the transversal direction over the whole device is correct. Rigorously speaking, the model refers to an ideal situation.
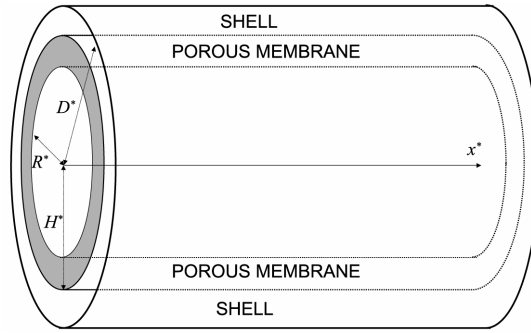
Figure 2. A single hollow fiber and the surrounding permeate flow region or shell.
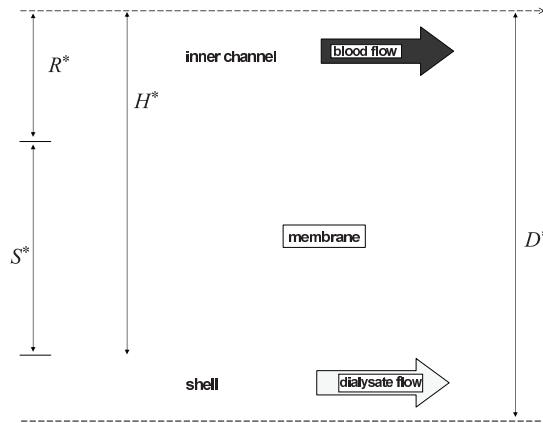

Figure 3. A schematic of the geometry at the fiber level.

- The inner channel, $\{0 < r^* < R^*, 0 < x^* < L^*\}$, where the blood flows.
- The porous membrane, $\{R^* < r^* < H^*, 0 < x^* < L^*\}$.
- The shell, or the permeate flow region, $\{H^* < r^* < D^*, 0 < x^* < L^*\}$, where the permeate and the synthetic dialyzate flow.

In practical cases the fiber thickness S^* is comparable to R^*, that is[4]

$$\frac{S^*}{R^*} = \mathcal{O}(1).$$

Small toxic compounds such as urea or low molecular weight proteins can permeate through the membrane but, on the other hand, cells and proteins

---

[4] By $\mathcal{O}(1)$ we mean a quantity well separated from ε and $1/\varepsilon$. A similar convention is adopted for other orders.

Quantity	Typical Range	Selected Value	Units	Source of Data
R^*	10^{-2}	10^{-2}	cm	[28], [15]
L^*	$20 \div 30$	25	cm	[28], [15]
S^*	$0.2 \div 0.5 \times 10^{-2}$	0.4×10^{-2}	cm	[28], [15]
D^*	$2 \div 2.5 \times 10^{-2}$	2.3×10^{-2}	cm	[28], [15]
$\frac{D^*-H^*}{R^*}$	$0.5 \div 1.3$	0.9		
ε	$10^{-4} \div 10^{-3}$	4×10^{-4}		
$\mathcal{N}$	10^4	10^4		[49]
K^*	$10^{-14} \div 10^{-12}$	10^{-12}	cm^2	[28], [15]
V_b^*	$7 \div 8 \times 10^{-2}$	$7.9 \cdot 10^{-2}$	lt	[28], [15]

Table 1. Typical geometrical and physical values. In particular, for $\mathcal{N}$, number of fibers in the dialyzer, we refer to [49]. $V_b^* = \pi \mathcal{N} R^{*2} L^*$, denotes the total blood volume contained in the fibers boundle.

(e.g. the albumin molecular weight is ∼66.5 KDa) cannot permeate. Actually the membrane inner interface is coated by a layer (whose thickness depends on the longitudinal coordinate and varies in time) of proteins (see, e.g., [1]). Albumin, accumulating on the membrane surface, causes membrane fouling and lumen reduction as well. In a first instance we disregard such a phenomenon.

The shell thickness $(D^* - H^*)$, is comparable with the inner channel radius, namely

$$\frac{D^* - H^*}{R^*} = \mathcal{O}(1).$$

In Table 1 we have reported the dialyzers typical characteristics.

The membrane, see Fig. 3, is modeled as a uniform and isotropic porous medium and the flow here occurring is Darcian. We denote by K^*, $[K^*] = $ cm^2, the membrane permeability, and assume K^* uniform and constant[5]. The range of K^* is reported in Table 1. The flow through the membrane is driven by the pressure difference locally established between the channel and the shell (the so-called transmembrane pressure, TMP). Actually, an oncotic pressure, opposing the outflow, is present between the inner channel and the shell, with a negative contribution to TMP. We shall return to such an important issue in the sequel.

Concerning blood, we model it as a two-components mixture[6]: (i) plasma, index "$_{pl}$", the fluid component; and (ii) cells, mainly Red Blood Cells[7], index

---

[5] Recall we are neglecting any membrane fouling phenomena.

[6] We refer the reader to [7], [38] for the continuum mechanics approach to mixtures.

[7] White blood cells, which can be of different species, are larger than RBC's, but by far less numerous. Platelets, much smaller than RBC's, occupy a very small volume fraction.

"$_{RBC}$". The RBC's volume fraction, usually referred to as hematocrit, is denoted by ϕ.

The plasma is a solution consisting of:

Solvent: liquid (serum).
Solutes: low molecular weight components (e.g. urea) and large molecular weight protein (mainly serum-albumin). Hence, we introduce:

– $\hat{c}_i^*$, $i = 1, \dots, N$, $[\hat{c}_i^*]$ = gr/dl, the concentration of the ith low molecular compound in the plasma (mass per plasma unit volume). All of them can permeate through the membrane.
– $\hat{c}_p^*$, $[\hat{c}_p^*]$ = gr/dl, the concentration of in the plasma (total mass of per plasma unit volume). They cannot permeate through the membrane.
– c_β^*, $\beta = p, 1, \dots, N$, the concentration of the βth solute in the whole blood (mass of the βth solute per blood unit volume). We have

$$(2.1) \qquad\qquad c_\beta^* = (1 - \phi)\hat{c}_\beta^*, \quad \beta = p, 1, \dots, N.$$

The two mixture components (plasma and RBC's) have essentially the same density ρ^*, constant (typically $\rho^* \approx 1$ gr/cm^3). Actually we neglect the influence of the chemical composition on blood density. This allows to focus on the fluid dynamic problem, which can be analyzed independently of the removal of chemicals from the fluid.

We denote by:

• $\vec{v}_\alpha^*$, $\alpha = pl$, RBC, the velocity of the αth blood component within the channel.
• $\vec{v}^*$, the velocity of blood as a whole (i.e. of the mixture). In particular, according to [7], [38], we have

$$(2.2) \qquad\qquad \vec{v}^* = (1 - \phi)\vec{v}_{pl}^* + \phi\vec{v}_{RBC}^*.$$

• $\vec{q}^*$, the specific discharge within the membrane.
• $\vec{w}^*$, the permeate velocity, i.e. the fluid velocity in the shell.

From the rheological point of view we consider blood to be a non-Newtonian shear-thinning fluid (see [32] and also [33], [47]), whose Cauchy stress is

$$(2.3) \qquad\qquad \mathbf{T}^* = -p_{ch}^*\mathbf{I} + 2\mu_{blood}^*\left[1 + \frac{5}{2}\phi\gamma(II_{\mathbf{D}^*}^*)\right]\mathbf{D}^*,$$

where:

• $\mathbf{D}^* = 1/2(\nabla^*\vec{v}^* + (\nabla^*\vec{v}^*)^{\mathrm{T}})$, is the symmetric part of the velocity gradient. ∇^* denotes the gradient operator with respect to space coordinates x^*, r^*, and $(\cdot)^{\mathrm{T}}$ is the transposed matrix.
• p_{ch}^*, is the pressure in the channel.
• $II_{\mathbf{D}^*}^* = \sqrt{1/2\,\mathrm{tr}(4\mathbf{D}^{*2})}$, with $\mathrm{tr}(\cdot)$ denoting the trace operator, [33].

- μ_{blood}^* is the blood viscosity, for which we choose the constitutive equation [34]

$$(2.4) \qquad \mu_{blood}^* = \mu_{ref}^* \lambda(\hat{c}_p),$$

with μ_{ref}^*, viscosity reference value (see Table 2),

$$(2.5) \qquad \lambda(\hat{c}_p) = \lambda_1 + \lambda_2 \hat{c}_p,$$

with λ_1, λ_2, reported in Table 2, and

$$(2.6) \qquad \hat{c}_p = \frac{\hat{c}_p^*}{\hat{c}_{p,ref}^*},$$

where $\hat{c}_{p,ref}^*$ is the reference value for the protein concentration within the plasma (see Table 2).
- $\gamma(II_{\mathbf{D}^*}^*)$ is a given function. Here we consider a shear-thinning model obtained combining the one analyzed in [6] with the one presented in [37], and well summarized in [15], namely[8]

$$(2.7) \qquad \gamma(II_{\mathbf{D}^*}^*) = \frac{1}{(1 + \beta^* II_{\mathbf{D}^*}^*)^n},$$

where β^*, and n, are parameters to be selected according to experimental data. Many other models have been proposed (see, e.g., [35] or [52], [33], [11], [23], [47] and [36]), but the choice of the rheology is not so critical in the present context.

Concerning the dialyzate flow in the in shell, we model it as an incompressible Newtonian fluid, whose Cauchy stress is

$$\mathbf{T}^* = -p_s^* \mathbf{I} + 2\mu_{H_2O}^* \mathbf{D}_w^*,$$

where $\mathbf{D}_w^* = 1/2(\nabla^* \vec{w}^* + (\nabla^* \vec{w}^*)^{\mathrm{T}})$, p_s^* denotes the pressure within the shell and $\mu_{H_2O}^*$, is the water viscosity (see Table 2). Due to the incompressibility constraint we have

$$(2.8) \qquad \mathrm{tr}(\mathbf{D}_w^*) = 0.$$

The flows in the channel and in the shell are both driven by the following prescribed pressures (see Table 2 for typical values):

– inlet ($x^* = 0$) channel pressure: $p_{ch,in}^*$;
– outlet ($x^* = L^*$) channel pressure: $p_{ch,out}^*$;
– inlet ($x^* = 0$) shell pressure: $p_{s,in}^*$;
– outlet ($x^* = L^*$) shell pressure: $p_{s,out}^*$.

---

[8] Formula (2.7) satisfies the invariance properties since it involves only frame invariant quantities.
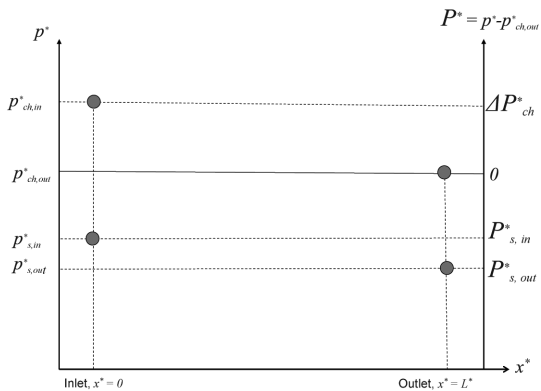
Figure 4. Pressure levels (not on scale).

The fluid pressure in the membrane is denoted by p_m^*. Next we set

$$(2.9) \qquad\qquad P_a^* = p_a^* - p_{ch,out}^*, \quad a = ch, m, s,$$

so that the outlet channel (rescaled) pressure is 0. For the time being we consider $p_{ch,in}^*$, $p_{ch,out}^*$, $p_{s,in}^*$, and $p_{s,out}^*$, constant in time, but minor changes allow to introduce time dependence[9]. We note that, in practice, $p_{ch,out}^*$ is the patient's blood pressure in the receiving vessel. A schematic representation of the pressure levels is shown in Fig. 4, and reported in Table 2 for the specific case of concordant flows[10].

We remark that in place of using heuristic formulas for the transmembrane discharge, like the one known as Starling hypothesis [48], frequently adopted in the context of blood filtration, our model incorporates the full analysis of the cross flow.

The size of some of the proteins carried in the blood (mainly albumin) is in the range to produce a non-negligible oncotic pressure[11] Π^*. Hence, following [30], sect. 2, vol. II, chapt. 29, p. 961–1034, we use the Landis-Pappenheimer law

$$(2.10) \qquad \Pi^*(\hat{c}_p^*) = A_1^* \hat{c}_p^* + A_2^* \hat{c}_p^{*2} + A_3^* \hat{c}_p^{*3}, \quad [\Pi^*] = \text{mmHg},$$

with A_i^*, $i = 1, 2, 3$, reported in Table 3. Osmosis produces a pressure discontinuity at the inner channel walls, so that $p_{ch}^*|_{r^*=R^*} = p_m^*|_{r^*=R^*} - \Pi^*$, as we shall illustrate in section 6. The fact that $\hat{c}_p^*$ appears in (2.10) in place of c_p^* implies the assumption that the membrane is everywhere in contact with plasma.

---

[9] In such a case we keep the symbols $P_{ch,in}^*$, $P_{ch,out}^*$, $P_{s,in}^*$, and $P_{s,out}^*$, to denote the respective order of magnitude.

[10] The case of counterflow can be treated in a similar way.

[11] Oncotic pressure is osmotic pressure referred to colloids. Solutes whose molecules are small enough to be effectively transported across the membrane (i.e. the $j = 1, \ldots, N$, solutes) do not contribute to oncotic pressure, because of the particular composition of the dialysate.

Quantity	Typical Value	Units	Source of Data
μ_{ref}^*	1.22	cP	[34]
$\mu_{H_2O}^*$	1	cP	
$\mu = \mu_{ref}^*/\mu_{H_2O}^*$	1.22		
λ_1	0.82		[34]
λ_2	0.18		[34]
$\hat{c}_{p,ref}^*$	7	gr/dl	[28]
$\phi|_{x=0}$ (inlet)	$\phi_{in} = 0.4$		[28], [15]
$\phi|_{x=1}$ (outlet)	1.25 ϕ_{in}		[28], [15]
$p_{ch,in}^*$	125	mmHg	[28]
$p_{ch,out}^*$	85	mmHg	[28]
$p_{s,in}^*$	61	mmHg	[28]
$p_{s,out}^*$	59	mmHg	[28]

Table 2. Typical values for pressure (expressed in mmHg,—recall that 1 mmHg = 133.3 Pa = $1.333 \cdot 10^3$ dyn/cm^2), hematocrit, viscosity (recall 1 cP = 10^{-2} dyn s/cm^2), and protein concentration. Note that the inlet and outlet values of the hematocrit are considerably different due to the water loss along the fibers.

A_1^* mmHg (gr/dl)$^{-1}$	A_2^* mmHg (gr/dl)$^{-2}$	A_3^* mmHg (gr/dl)$^{-3}$
2.1	0.16	0.009

Table 3. Landis Pappenheimer oncotic pressure coefficients, [30].

3. SCALINGS

We use a double scaling for the spatial variables x^* and r^* (see Fig. 2)

(3.1)
$$x = \frac{x^*}{L^*}, \quad r = \frac{r^*}{\varepsilon L^*}.$$

We also introduce

$$D = \frac{D^*}{R^*}, \quad S = \frac{S^*}{R^*}, \quad H = \frac{H^*}{R^*},$$

which are all $\mathcal{O}(1)$ (see Table 1).

Next, we introduce v_{ref}^*, the characteristic longitudinal blood velocity and q_{ref}^*, the characteristic specific cross discharge (typical values are reported in Table 4), defined according to formulas (3.14), (3.15), below.

The characteristic convection time is

$$(3.2) \qquad t_{ref}^* = \frac{L^*}{v_{ref}^*},$$

and we select it as reference time scale (see again Table 4), so that $t = t^*/t_{ref}^*$, is the dimensionless time variable.

Next, we adopt the double rescaling for velocities

$$(3.3) \qquad v_x = \frac{v_x^*}{v_{ref}^*}, \quad \text{and} \quad v_{\alpha,x} = \frac{v_{\alpha,x}^*}{v_{ref}^*}, \quad \alpha = pl, RBC,$$

$$(3.4) \qquad v_r = \frac{v_r^*}{\varepsilon v_{ref}^*}, \quad \text{and} \quad v_{\alpha,r} = \frac{v_{\alpha,r}^*}{\varepsilon v_{ref}^*}, \quad \alpha = pl, RBC.$$

The flux within the membrane is rescaled as

$$(3.5) \qquad q_x = S\varepsilon \frac{q_x^*}{q_{ref}^*}, \quad \text{and} \quad q_r = \frac{q_r^*}{q_{ref}^*}.$$

Thus we have $\vec{q}^* = q_{ref}^* \left(\frac{1}{S\varepsilon} q_x \vec{e}_x + q_r \vec{e}_r \right)$.

We denote by w_{ref}^*, the characteristic longitudinal fluid velocity in the shell (see formula (3.20) below), and define

$$(3.6) \qquad w_x = \frac{w_x^*}{w_{ref}^*}, \quad \text{and} \quad w_r = \frac{w_r^*}{\varepsilon w_{ref}^*}.$$

The characteristic pressure drop (see also Fig. 4) along the fiber is

$$(3.7) \qquad \Delta P_{ch}^* = p_{ch,in}^* - p_{ch,out}^* > 0,$$

and, recalling (2.9), we introduce the dimensionless rescaled pressures

$$P_a = \frac{P_a^*}{\Delta P_{ch}^*} = \frac{p_a^* - p_{ch,out}^*}{\Delta P_{ch}^*}, \quad a = ch, m, s.$$

In a parallel way we set $\Delta P_s^* = p_{s,in}^* - p_{s,out}^* > 0$, and

$$P_{s,in} = \frac{p_{s,in}^* - p_{ch,out}^*}{\Delta P_{ch}^*}, \quad P_{s,out} = \frac{p_{s,out}^* - p_{ch,out}^*}{\Delta P_{ch}^*}.$$

Finally

$$(3.8) \qquad \Delta P_{TM} = \frac{1}{\Delta P_{ch}^*} \left(\frac{p_{ch,in}^* + p_{ch,out}^*}{2} - \frac{p_{s,in}^* + p_{s,out}^*}{2} \right) > 0,$$

Quantity	Exper. Value	Units	Source of Data	Estimated Value (Formula)
v_{ref}^*	$1 \div 2$	cm/s	[28]	2 (3.14)
w_{ref}^*	~ 2	cm/s	[28]	3.8 (3.20)
q_{ref}^*	$10^{-3} \div 10^{-4}$	cm/s	[28]	1.5×10^{-3} (3.15)
t_{ref}^*	$12 \div 25$	s	[28]	12 (3.2)
Os				0.37 (3.13)
ΔP_s^*	2	mmHg	[28]	
ΔP_{ch}^*	40	mmHg	[28]	
Π_{ref}^*		mmHg		14.7 (3.11)
ΔP_{TM}				1.12 (3.8)
$P_{s,in}$				-0.6 (3.10)
$P_{s,out}$				-0.65 (3.10)

Table 4. We remark that the measured value of v_{ref}^*, q_{ref}^*, and w_{ref}^*, reported in the table agrees with the ones obtained by formulas (3.14), (3.15) and (3.20), respectively. The ratio between the blood velocity and the typical cross discharge can be considered $\mathscr{O}(\varepsilon)$, in agreement with (3.16). The estimated values are computed using the selected values reported in Tables 2 and 1.

giving the average TMP (scaled with ΔP_{ch}^*). We refer to Table 4 for the typical values of reference quantities.

We thus have:

- Inner channel

$$(3.9) \qquad \begin{cases} \text{inlet: } P_{ch}|_{x=0} = 1, \\ \text{outlet: } P_{ch}|_{x=1} = 0. \end{cases}$$

- Outer shell (see Table 4 for typical values)

$$(3.10) \qquad \begin{cases} \text{inlet: } P_s|_{x=0} = P_{s,in}, \\ \text{outlet: } P_s|_{x=1} = P_{s,out}. \end{cases}$$

Concerning the oncotic pressure, we rescale it with (see Table 4)

$$(3.11) \qquad \Pi_{ref}^* = A_1^* \hat{c}_{p,ref}^*.$$

Thus, recalling (2.6), we may write

$$(3.12) \qquad \Pi^* = \Pi_{ref}^* \hat{\Pi}(\hat{c}_p), \quad \text{with } \hat{\Pi}(\hat{c}_p) = \hat{c}_p + B_1 \hat{c}_p^2 + B_2 \hat{c}_p^3,$$

with B_1, and B_2, given in Table 5.

$B_1 = \dfrac{A_2^* \hat{c}_{p,ref}^*}{A_1^*}$	$B_2 = \dfrac{A_3^* c_{p,ref}^{*2}}{A_1^*}$
0.53	0.21

Table 5. Values of B_1 and B_2, in (3.12).

Next, we introduce the characteristic number

$$(3.13) \qquad\qquad \mathsf{Os} = \frac{\Pi_{ref}^*}{\Delta P_{ch}^*},$$

measuring the importance of the oncotic pressure w.r.t. the hydraulic pressure. In general $\mathsf{Os} \lesssim 1$ (see, e.g., Table 4).

The reference longitudinal velocity in the cannel, v_{ref}^*, is estimated recalling the Poiseuille flow in a tube of radius R^*. We thus set

$$(3.14) \qquad\qquad v_{ref}^* = \frac{\Delta P_{ch}^*}{8\mu_{ref}^* L^*} R^{*2}.$$

Concerning the characteristic discharge within the membrane, i.e. q_{ref}^*, we define it exploiting Darcy's law, in which we take $\Delta P_{TM}\Delta P_{ch}^*$ as average trans-membrane pressure, namely

$$(3.15) \qquad\qquad q_{ref}^* = \frac{K^*}{\mu_{H_2O}^*} \frac{\Delta P_{TM}\Delta P_{ch}^*}{SR^*}.$$

In particular, recalling (3.14) we have

$$(3.16) \qquad\qquad \frac{q_{ref}^*}{v_{ref}^*} = \varepsilon\mu\mathsf{G}\Delta P_{TM},$$

with (see Table 2)

$$(3.17) \qquad\qquad \mu = \frac{\mu_{ref}^*}{\mu_{H_2O}^*},$$

and

$$(3.18) \qquad\qquad \mathsf{G} = \frac{8K^* L^{*2}}{SR^{*4}} = \frac{8}{\varepsilon^2 S}\mathsf{Da},$$

where

$$(3.19) \qquad\qquad \mathsf{Da} = \frac{K^*}{R^{*2}},$$

G	Da	F	q_{ref}^*/v_{ref}^*
$0.1 \div 10$	$10^{-10} \div 10^{-8}$	0.8	$10^{-5} \div 10^{-4}$

Table 6. Typical values for G, Da, F, and q_{ref}^*/v_{ref}^*.

Q_{in}^* [ml/min]	Q_{TM}^* [ml/min]	$\mathfrak{F}$
200	1.6	$\sim 10^{-2}$

Table 7. In some cases $Q_{TM}^* \sim 20$ ml/min, so that $\mathfrak{F} \sim 10^{-1}$. Recall that 1 ml = 1 cm^3.

is the so-called Darcy's number (see Table 6 for typical values. Parametr F defined in (3.21) below).

We introduce two more references quantities: the overall blood inlet discharge Q_{in}^* and the overall plasma transmembrane (or lateral) discharge Q_{TM}^*. We have

$$Q_{in}^* = \mathcal{O}(\mathcal{N}\pi R^{*2}v_{ref}^*), \quad Q_{TM}^* = \mathcal{O}(2\pi\mathcal{N}R^*L^*q_{ref}^*),$$

where $\mathcal{N}$ is the number on fibers in the dialyzer (see Table 2). The ratio

$$\mathfrak{F} = \frac{Q_{TM}^*}{Q_{in}^*},$$

in usual operating conditions is $\sim 10^{-2}$ (see Table 7).

Actually the selection of an appropriate reference value for Q_{TM}^*, is a rather delicate issue. Indeed, assuming Q_{TM}^* simply proportional (via the total fibers surface) to the Darcy's discharge, it is equivalent to neglect backfiltration. The latter is an important phenomena which, in certain circumstances, may even counterbalance the outflow. So, taking $Q_{TM}^* \sim 2\pi\mathcal{N}R^*L^*q_{ref}^*$, may lead to a large overestimation of the actual lateral discharge. Hence, $2\pi\mathcal{N}R^*L^*q_{ref}^*$, represents an upper bound for the lateral flow, rather than a characteristic value. The resulting estimate of $\mathfrak{F}$, is therefore an estimate of the maximum value of the ratio between the lateral and inlet discharge.

Next, exploiting the basic formula of Poiseuille flow in an annulus, we define the reference permeate velocity

$$(3.20) \qquad w_{ref}^* = \frac{\Delta P_s^*}{\mu_{H_2O}^* L^*} R^{*2}(D^2 - H^2) = \mu v_{ref}^* F,$$

where μ is given by (3.17) and

$$(3.21) \qquad F = 8\frac{\Delta P_s^*}{\Delta P_{ch}^*}(D^2 - H^2).$$

We refer to Table 6 for a typical value of F.

4. THE MATHEMATICAL MODEL

To model the complex flow dynamics occurring in the structure, we have to analyze separately the three different regions and then we impose the coupling boundary conditions at the interfaces. We end up with this integro-differential model governing the evolution of the various unknown in the dialyzer

$$(4.1) \quad \begin{cases} \dfrac{\lambda(\hat{c}_p)}{8}\left(1 + \dfrac{5}{2}\phi\gamma\left(\dfrac{\partial v_x}{\partial r}\right)\right)\dfrac{\partial v_x}{\partial r} = -\dfrac{r}{2}\left(-\dfrac{\partial P_{ch}}{\partial x} + \mathsf{R_p}g_x\right), \\[2mm]
v_x|_{r=1} = -\dfrac{1}{\mathsf{B}}\dfrac{\partial v_x}{\partial r}\bigg|_{r=1}, \\[2mm]
\displaystyle\int_0^1 r\dfrac{\partial v_x}{\partial x}\,dr = \dfrac{\mu \mathsf{SG}}{\ln H}(P_s - P_{ch} + \mathsf{Os}\,\hat{\Pi}(\hat{c}_p)), \\[2mm]
P_{ch}|_{x=0} = 1, \quad P_{ch}|_{x=1} = 0, \\[2mm]
\dfrac{\partial^2 P_s}{\partial x^2} = \dfrac{\mathsf{G}}{\mathfrak{R}_0}[P_s - P_{ch} + \mathsf{Os}\,\hat{\Pi}(\hat{c}_p)], \\[2mm]
P_s(x=0) = P_{s,in}, \quad P_s(x=1) = P_{s,out}, \\[2mm]
\dfrac{1}{\phi}\dfrac{D\phi}{Dt} = 2\dfrac{\mu \mathsf{SG}}{\ln H}(P_{ch} - P_s - \mathsf{Os}\,\hat{\Pi}(\hat{c}_p)) \\[2mm]
\phi|_{x=0} = \phi_{in}(t), \\[2mm]
\dfrac{1}{\hat{c}_p}\dfrac{D\hat{c}_p}{Dt} = \dfrac{2}{1-\phi}\dfrac{\mu \mathsf{SG}}{\ln H}(P_{ch} - P_s - \mathsf{Os}\,\hat{\Pi}(\hat{c}_p)), \\[2mm]
\dfrac{1}{\hat{c}_i}\dfrac{D\hat{c}_i}{Dt} = -2\mathfrak{D}_i\left(1 - \dfrac{\mathfrak{r}_i^{(d)}}{\hat{c}_i}\right), \\[2mm]
\hat{c}_p|_{x=0} = \hat{c}_{p,in}(t), \quad \hat{c}_i|_{x=0} = \hat{c}_{i,in}(t), \quad i = 1, 2, \ldots, N,
\end{cases}$$

where

$$(4.2) \qquad\qquad \mathsf{R_P} = \dfrac{\rho^* g^* L^*}{\Delta P_{ch}^*},$$

$\mathfrak{D}_i$, $i = 1, 2, \ldots N$, is the dimensionless diffusion of the ith low molecular compound (see (6.35) in Appendix A). Concerning the other dimensionless parameters $\mathfrak{R}_0$, B, and $\mathfrak{r}_i^{(d)}$ appearing in (4.1), as well as its detailed derivation, we refer to Appendix A. Here we just list the three assumptions that we considered for the derivation (4.1).

ASSUMPTION 1. *Since the fiber radius is of the order of a few RBC's diameters, the flow conditions are such that, from the very beginning, we have:*

- $\phi = \phi(x, t)$, as a consequence of efficient RBC's radial dispersion.
- $v^*_{RBC,r} \equiv 0$, consistently with the fairly uniform radial distribution of the RBC's and with the fact that RBC's do not cross the membrane.
- The RBC's diffusive longitudinal velocity with respect to blood is negligible. Hence $v^*_{RBC,x} = v^*_x$.

ASSUMPTION 2. *Proteins are uniformly distributed over the fiber cross section, namely $\hat{c}^*_p = \hat{c}^*_p(x, t)$.*

ASSUMPTION 3. *Solutes are uniformly distributed over the fiber cross section $\hat{c}_i = \hat{c}_i(x, t)$, $i = 1, \ldots, N$.*

We stress that the inlet values $\phi_{in}(t)$, $\hat{c}_{p,in}(t)$, and $\hat{c}_{i,in}(t)$, $i = 1, 2, \ldots, N$, are actually unknown. Their determination requires the coupling of the system above with the solutes dynamics and water redistribution taking place in the patient's body, considered as a separate compartment. This task will be carried out in the next section.

5. INLET CONDITIONS FOR THE HEMATOCRIT ϕ, AND FOR THE SOLUTES CONCENTRATIONS

We follow [14], considering a two-compartment model: intracellular and extracellular. Other models (see for instance [27] or [19] and the literature therein) consider a further division of the extracellular compartment in: interstitial and blood sub-compartments. Such an approach is certainly appealing, but requires a constitutive equation for fluid and mass exchange rate between the interstices and blood sub-compartments[12], leading to a considerable increase of the number of unknowns and equations. On the contrary, models like [14] have the advantage of simplicity, though they miss the information on how water is exchanged between interstices and blood. In the present approach we will bypass this difficulty by assuming, that:

ASSUMPTION 4. *The inlet hematocrit is constant. So, recalling* (6.50),

$$(5.1) \qquad \qquad \phi_{in}(t^*) = \phi_o.$$

Accordingly, since the total mass of "large proteins" in the patient's plasma does not vary during the continuous renal replacement therapy (CRRT), the inlet protein concentration is also constant. Hence, setting $\hat{c}^*_{p,in} = \hat{c}^*_{p,ref}$, we have

$$(5.2) \qquad \qquad \hat{c}_{p,in} = 1 \quad \forall t \geq 0, \quad and \quad \hat{c}_p(x, 0) = 1.$$

---

[12] In [54] the problem is analyzed considering also the difference between the blood pressure at the arterial and venous capillaries.
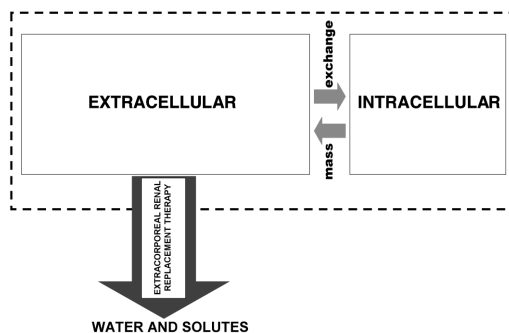
Figure 5. A schematic representation of a compartments model [14].

From the physical point of view, the above assumption means that the refilling process (occurring from interstices to blood) is faster than the average outlet-to-inlet blood circulation time (order of few min).

The dynamics of the water stored/consumed in the body is schematically represented in Fig. 5.

Following [14], we introduce:

- $M_{U,ic}^*(t^*)$, total mass of urea in the intracellular compartment.
- $M_{U,ec}^*(t^*)$, total mass of urea in the extracellular compartment.
- $M_{Na,ec}^*(t^*)$, total mass of Na in the extracellular compartment.
- $V_{ec}^*(t^*)$, $V_{ic}^*(t^*)$, the volume of water stored, at time t^*, in the extracellular compartment (namely in the blood and in the interstitial space), and in the intracellular compartment, respectively.

The solutes inlet concentrations are the ones in the extracellular compartment, namely

$$(5.3) \qquad \hat{c}_{i,in}^*(t^*) = \frac{M_{i,ec}^*(t^*)}{V_{ec}^*(t^*)}, \quad i = \text{U, Na.}$$

As stated in [14], the redistribution of fluid and solutes between the compartments has to fulfill the requirement of osmotic equilibrium, namely

$$(5.4) \qquad \frac{M_{Na,ec}^*(t^*) + M_{U,ec}^*(t^*) + M_{eq,ec}^*}{V_{ec}^*(t^*)} = \frac{M_{U,ic}^*(t^*) + M_{eq,ic}^*}{V_{ic}^*(t^*)},$$

where $M_{eq,ic}^*$, and $M_{eq,ec}^*$, represent the equivalent mass of all other solutes generating osmosis in the intracellular and extracellular compartment, respectively. Still according to [14] they do not change significantly during the treatment. In particular, $M_{eq,ec}^* = C_{eq,ec}^*(0)V_{ec}^*(0)$, where $C_{eq,ec}^*(0)$ is the initial concentration in the extracellular compartment (see Table 8) and $V_{ec}^*(0)$ is the initial volume of the water stored in the extracellular compartment. The latter can be estimated in

terms of the total initial volume of water stored in the body $V_T^*(0)$. In particular, (see Table 8 and [14])

$$(5.5) \qquad \frac{V_{ic}^*(0)}{V_T^*(0)} = \frac{5}{8}, \quad \text{and} \quad \frac{V_{ec}^*(0)}{V_T^*(0)} = \frac{3}{8}$$

Concerning $M_{eq,ic}^*$, we assume that, at the initial time the urea concentration in the extracellular and in the intracellular compartment are equal, that is (in Table 8 we have reported the typical value of $M_{U,ec}^*(0)/V_{ec}^*(0)$)

$$(5.6) \qquad \frac{M_{U,ec}^*(0)}{V_{ec}^*(0)} = \frac{M_{U,ic}^*(0)}{V_{ic}^*(0)}, \quad \underset{(5.5)}{\Rightarrow} \quad M_{U,ic}^*(0) = \frac{5}{3} M_{U,ec}^*(0).$$

Hence

$$(5.7) \qquad M_{eq,ic}^* = \frac{5}{3} M_{Na,ec}^*(0) \left(1 + \frac{M_{eq,ec}^*}{M_{Na,ec}^*(0)} \right).$$

The solute masses vary because of the exchange that takes place between the compartments, and because of the extraction (ultrafiltration) and generation (metabolism). Hence, considering the total fluid mass balance, [14] we can write

$$(5.8) \quad \begin{cases} \dfrac{d}{dt^*}[V_{ec}^*(t^*) + V_{ic}^*(t^*)] = -\dot{\mathscr{R}}^* \\[2mm] \dfrac{dM_{U,ic}^*(t^*)}{dt^*} = -K_U^* V_T^*(0) \left(\dfrac{M_{U,ic}^*(t^*)}{V_{ic}^*(t^*)} - \dfrac{M_{U,ec}^*(t^*)}{V_{ec}^*(t^*)} \right), \\[2mm] \dfrac{dM_{U,ec}^*(t^*)}{dt^*} = K_U^* V_T^*(0) \left(\dfrac{M_{U,ic}^*(t^*)}{V_{ic}^*(t^*)} - \dfrac{M_{U,ec}^*(t^*)}{V_{ec}^*(t^*)} \right) + \mathscr{G}_U^* - \mathfrak{I}_U^*, \\[2mm] \dfrac{dM_{Na,ec}^*(t^*)}{dt^*} = \mathscr{G}_{Na}^* - \mathfrak{I}_{Na}^*, \end{cases}$$

where V_{ex}^* is given by (5.4), and where:

- $\dot{\mathscr{R}}^*$, is the net water extraction rate[13]

$$(5.9) \qquad \dot{\mathscr{R}}^*(t^*) = 2\pi R^* \mathscr{N} \int_0^{L^*} v_r^*|_{r^*=R^*} \, dx^* - Q_r^*,$$

---

[13] We recall that, focussing on a single fiber, the lateral plasma discharge is proportional to $(1-\phi)v_{pl,r}^*|_{r^*=R^*}$, or, exploiting (6.17)$_2$, to $v_r^*|_{r^*=R^*}$.

Parameter	Value	Units	Source of data
$V_{ec}^*(0)$	$\frac{3}{8}V_T^*(0)$	lt	[20]
$V_{ic}^*(0)$	$\frac{5}{8}V_T^*(0)$	lt	[20]
$M_{eq,ec}^*(0)/V_{ec}^*(0)$	6	mEq/lt	[43], [20]
$M_{Na,ec}^*(0)/V_{ec}^*(0)$	140	mEq/lt = mmol/lt	[14]
$M_{U,ec}^*(0)/V_{ec}^*(0)$	10	mmol/lt	[14]
$M_{eq,ic}^*(0)/V_{ec}^*(0)$	243.3	mmol/lt	
$K_U^* V_T^*(0)$	0.77	lt/min	[14], [27]
$V_T^*(0)$	40	lt	[14]
K_U^*	0.018	min^{-1}	[14], [27]
$\mathscr{G}_U^*$	0.075	mmol/min	[14]
$\mathscr{G}_{Na}^*$	0.107	mEq/min	[14]

Table 8. Compartments model data. Concerning $M_{U,ec}^*(0)/V_{ec}^*(0)$, and $M_{Na,ec}^*(0)/V_{ec}^*(0)$, we refer to Table 10 and to formula (5.11). Next, $M_{eq,ic}^*(0)/V_{ec}^*(0)$, has been computed referring to Na$^+$moles.

where $\mathscr{N}$ is number of fibers in the hemodiafilter[14] (see Table 1) and Q_r^* is the replacement fluid flow rate. Actually, dialyzers operating in a "fast" regime (i.e. with a relatively large transmembrane flow) are equipped with a device (see, e.g. [39]) which may inject some plasma-like fluid into the blood just before it is returned to the patient's vein[15].

- K_U^*, is the urea mass transfer rate between the intracellular and extracellular compartments Table 8.
- $\mathscr{G}_i^*$, $i = $ U, Na, is the generation rate of the ith solute (see Table 8).
- $\mathfrak{J}_i^*$, $i = $ U, Na, is the solute extraction rate due to the dialyzer, that is

$$\mathfrak{J}_i^*(t^*) = 2\pi R^* \mathscr{N} \left[\int_0^{L^*} (\text{TOTAL OUTFLUX})_i \, dx^* \right].$$

---

[14] For the moment we assume that the filtration rate is the same for all the fibers. Formula (5.9) can be corrected introducing a non-uniform distribution of the driving pressures.

[15] The target value fluid removal may be reached before urea, creatinine, etc., have attained the desired concentrations. In that case two options are possible: (i) a flux $Q_r^* \simeq Q^*$, will be necessary to stabilize the hematocrit value; or (ii) a flux $Q_r^* = 0$, but the device operates in condition such that $\int_0^{L^*} v_r^*|_{r^*=R^*} \, dx^* = 0$. The selection of the most appropriate strategy is a delicate task of the operator.

Concerning $\dot{\mathscr{R}}^*(t^*)$, we introduce the total volume of the fibers (see also Table 1)

$$(5.10) \qquad\qquad V_b^* = \pi R^{*2} L^* \mathscr{N},$$

and recall (6.61), so that

$$\dot{\mathscr{R}}^*(t^*) = \frac{V_b^*}{t_{ref}^*} \left[2 \int_0^1 \frac{\mu SG}{\ln H} (P_{ch} - P_s - \mathsf{Os}\,\hat{\Pi}(\hat{c}_p))\, dx - Q_r \right],$$

where

$$Q_r = \frac{t_{ref}^*}{V_b^*} Q_r^*.$$

Next, for what $\mathfrak{J}_i^*$, $i = $ U, Na, is concerned we exploit (6.65), (6.67), (6.17)$_2$, (6.35) and (6.61) so to get

$$\mathfrak{J}_i^*(t^*) = 2\pi R^* \mathscr{N} \int_0^{L^*} (\mathscr{I}_{i,conv}^* + \mathscr{I}_{i,diff}^*)\, dx^*$$

$$= 2 \frac{V_b^* \hat{c}_{i,ref}^*}{t_{ref}^*} \left\{ \int_0^1 \hat{c}_i \left[\frac{\mu SG}{\ln H} (P_{ch} - P_s - \mathsf{Os}\,\hat{\Pi}(\hat{c}_p)) + (1-\phi)\mathfrak{D}_i \right] dx \right.$$

$$\left. - \mathfrak{D}_i \mathfrak{r}_i^{(d)} \int_0^1 (1-\phi)\, dx \right\},$$

with $\mathfrak{r}_i^{(d)}$ given by (6.36) and V_b^* by (5.10).

The inlet quantities to be inserted into system (4.1) are ϕ_{in} given by (5.1), $\hat{c}_{p,in}$ given by (5.2), and $\hat{c}_{i,in}$, $i = $ U, Na, given by (5.3). The mathematical formulation of the model, at the ε^0 order approximation, is now completed.

Let us now define the dimensionless quantities in a way that their initial value is 1. We thus set

$$V_{ic}(t) = \frac{V_{ic}^*(t)}{V_{ic}^*(0)} = \frac{V_{ic}^*(t)}{\frac{5}{8} V_T^*(0)}, \qquad V_{ec}(t) = \frac{V_{ec}^*(t)}{V_{ec}^*(0)} = \frac{V_{ec}^*(t)}{\frac{3}{8} V_T^*(0)}.$$

and

$$M_{U,ec}(t) = \frac{M_{U,ec}^*(t^*)}{M_{U,ec}^*(0)}, \qquad M_{U,ic}(t) = \frac{M_{U,ic}^*(t^*)}{M_{U,ic}^*(0)},$$

$$M_{Na,ec}(t) = \frac{M_{Na,ec}^*(t^*)}{M_{Na,ec}^*(0)}.$$

We are thus in position to define the reference values for the urea and Na plasma concentrations (see Table 10), namely

$$(5.11) \quad \hat{c}^*_{U,ref} = \frac{M^*_{U,ec}(0)}{V^*_{ec}(0)} = \frac{M^*_{U,ec}(0)}{\frac{3}{8} V^*_T(0)}, \quad \hat{c}^*_{Na,ref} = \frac{M^*_{Na,ec}(0)}{V^*_{ec}(0)} = \frac{M^*_{Na,ec}(0)}{\frac{3}{8} V^*_T(0)}.$$

Hence, recalling the definition (6.33) and formulas (5.3), (5.11), the inlet dimensionless concentrations are

$$(5.12) \qquad\qquad \hat{c}_{U,in}(t) = \frac{M_{U,ec}(t)}{V_{ec}(t)}, \quad \hat{c}_{Na,in}(t) = \frac{M_{Na,ec}(t)}{V_{ec}(t)}.$$

Next, taking (5.6)$_2$ into account, the dimensionless form of (5.4) is

$$(5.13) \qquad \frac{V_{ic}(t)}{V_{ec}(t)} [\mathscr{A}_1 M_{Na,ec}(t) + \mathscr{A}_2 M_{U,ec}(t) + \mathscr{A}_3] = \mathscr{A}_2 M_{U,ic}(t) + \frac{3}{5},$$

where the constants $\mathscr{A}_i$, $i = 1, 2, 3$, are specified in Table 9.

The dimensionless form of system (5.8) is the following

$\mathscr{A}_1$	$\dfrac{M^*_{Na,ec}(0)}{M^*_{eq,ic}}$	0.575
$\mathscr{A}_2$	$\dfrac{M^*_{U,ec}(0)}{M^*_{eq,ic}}$	0.11
$\mathscr{A}_3$	$\dfrac{M^*_{eq,ec}(0)}{M^*_{eq,ic}}$	0.025
$\mathscr{B}_1$	$K^*_U t^*_{ref}$	6×10^{-3}
$\mathscr{B}_2$	$\dfrac{V^*_b}{V^*_T(0)}$	2×10^{-3}
$\mathscr{G}_U$	$\dfrac{t^*_{ref}}{\mathscr{B}_1 M^*_{U,ec}(0)} \mathscr{G}^*_U$	2.6×10^{-2}
$\mathscr{G}_{Na}$	$\dfrac{t^*_{ref}}{\mathscr{B}_1 M^*_{Na,ec}(0)} \mathscr{G}^*_{Na}$	2.6×10^{-3}

Table 9. V^*_b has been taken from Table 1, while K^*_U, $M^*_{Na,ec}(0)/V^*_{ec}(0)$, $M^*_{U,ec}(0)/V^*_{ec}(0)$, $M^*_{eq,ec}(0)/V^*_{ec}(0)$, and $V^*_T(0) = 40$ lt, from Table 8. We have considered $t^*_{ref} = 20$ s. The expression of $M^*_{eq,ic}$, is given by formula (5.7). In computing A_2, we have considered the fact that $M^*_{eq,ic}$, refers to Na, while $M^*_{U,ec}$, to urea.

$$(5.14) \quad \begin{cases} \dfrac{1}{\mathscr{B}_1} \dfrac{d}{dt}\left[\dfrac{3}{8}V_{ec} + \dfrac{5}{8}V_{ic}\right] = -\dot{\mathscr{R}}, \\[2mm] \dfrac{1}{\mathscr{B}_1}\dfrac{dM_{U,ic}}{dt} = -\dfrac{8}{5}\left(\dfrac{M_{U,ic}}{V_{ic}} - \dfrac{M_{U,ec}}{V_{ec}}\right), \\[2mm] \dfrac{1}{\mathscr{B}_1}\dfrac{dM_{U,ec}}{dt} = \dfrac{8}{3}\left(\dfrac{M_{U,ic}}{V_{ic}} - \dfrac{M_{U,ec}}{V_{ec}}\right) + \mathscr{G}_U - \mathfrak{J}_U, \\[2mm] \dfrac{1}{\mathscr{B}_1}\dfrac{dM_{Na,ec}(t)}{dt} = \mathscr{G}_{Na} - \mathfrak{J}_{Na}, \end{cases}$$

where

$$(5.15) \qquad \dot{\mathscr{R}} = \dfrac{\mathscr{B}_2}{\mathscr{B}_1}\left[\int_0^1 2\dfrac{\mu SG}{\ln H}(P_{ch} - P_s - Os\,\hat{\Pi}(\hat{c}_p))\,dx - Q_r\right],$$

and

$$(5.16) \quad \mathfrak{J}_U = \dfrac{16}{3}\dfrac{\mathscr{B}_2}{\mathscr{B}_1}\int_0^1 \hat{c}_U\left[\dfrac{\mu SG}{\ln H}(P_{ch} - P_s - Os\,\hat{\Pi}(\hat{c}_p)) + (1 - \phi)\mathfrak{D}_U\right]dx,$$

$$(5.17) \qquad \mathfrak{J}_{Na} = \dfrac{16}{3}\dfrac{\mathscr{B}_2}{\mathscr{B}_1}\int_0^1 \hat{c}_{Na}\left[\dfrac{\mu SG}{\ln H}(P_{ch} - P_s - Os\,\hat{\Pi}(\hat{c}_p))\right.$$

$$\left. + (1 - \phi)\mathfrak{D}_{Na}\left(1 - \dfrac{r_{Na}^{(d)}}{\hat{c}_{Na}}\right)\right]dx,$$

and where the constants $\mathscr{B}_1$, $\mathscr{B}_2$, $\mathscr{G}_U$ and $\mathscr{G}_{Na}$ are defined in Table 9. We refer to Table 10 for the constant $r_{Na}^{(d)}$. In particular, (5.17) can be rewritten in a form that is easily "readable" from the physical point of view

$$\mathfrak{J}_{Na} = \underbrace{\dfrac{16}{3}\dfrac{\mathscr{B}_2}{\mathscr{B}_1}\int_0^1 \hat{c}_{Na}\left[\dfrac{\mu SG}{\ln H}(P_{ch} - P_s - Os\,\hat{\Pi}(\hat{c}_p))\right]dx}_{\text{convective flux}}$$

$$+ \underbrace{\dfrac{16}{3}\dfrac{\mathscr{B}_2}{\mathscr{B}_1}\int_0^1 (1 - \phi)\mathfrak{D}_{Na}(\hat{c}_{Na} - r_{Na}^{(d)})\,dx}_{\text{diffusive flux reduced by dialysate solutes}}.$$

The above system suggests the introduction of a new time scale, t^*_{comp}, characterizing the compartments dynamics, namely

$$(5.18) \qquad t^*_{comp} = \dfrac{t^*_{ref}}{\mathscr{B}_1}.$$

Hence, recalling the data in table 9, we get $t^*_{comp} \sim 156t^*_{ref}$, so that $t^*_{comp} = 30 \div 60$ min. Therefore, we introduce a new dimensionless time

$$(5.19) \qquad \tau = \frac{t^*}{t^*_{comp}}, \quad \Leftrightarrow \quad \tau = t\mathscr{B}_1,$$

so that $t = \mathcal{O}(1)$, means $\tau = 0(\mathscr{B}_1)$, while $\tau = \mathcal{O}(1)$, yields $t = \mathcal{O}(\mathscr{B}_1^{-1})$. Hence we rewrite system (5.14) and (5.13) in this way

$$(5.20) \quad \begin{cases} \dfrac{d}{d\tau}\left[\dfrac{3}{8}V_{ec} + \dfrac{5}{8}V_{ic}\right] = -\dot{\mathscr{R}}, \\[2ex] \dfrac{dM_{U,ic}}{d\tau} = -\dfrac{8}{5}\left(\dfrac{M_{U,ic}}{V_{ic}} - \dfrac{M_{U,ec}}{V_{ec}}\right), \\[2ex] \dfrac{dM_{U,ec}}{d\tau} = \dfrac{8}{3}\left(\dfrac{M_{U,ic}}{V_{ic}} - \dfrac{M_{U,ec}}{V_{ec}}\right) + \mathscr{G}_U - \mathfrak{I}_U, \\[2ex] \dfrac{dM_{Na,ec}(t)}{d\tau} = \mathscr{G}_{Na} - \mathfrak{I}_{Na}, \\[2ex] \dfrac{V_{ic}(t)}{V_{ec}(t)}\left[\mathscr{A}_1 M_{Na,ec}(t) + \mathscr{A}_2 M_{U,ec}(t) + \mathscr{A}_3\right] - \mathscr{A}_2 M_{U,ic}(t) - \dfrac{3}{5} = 0. \end{cases}$$

6. FINAL SIMPLIFIED MODEL AND NUMERICAL SIMULATIONS

We now operate two simplifications that reduce the complexity of the model, summarized as follows:

(S1) We select t^*_{comp}, given by (5.18), as reference time scale and neglect the local time evolution of ϕ, $\hat{c}_p$, and $\hat{c}_i$, during their transit within the dialyzer hollow fiber (in other words we consider a *quasi-stationary approximation*).

(S2) We consider a simplified rheological model, assuming that the blood behaves as a Newtonian fluid, whose viscosity depends on both: hematocrit and protein concentration. We thus rewrite (2.3) as

$$(6.1) \qquad \mathbf{T}^* = -p^*_{ch}\mathbf{I} + 2\mu^*_{blood}\left(1 + \frac{5}{2}\phi\right)\mathbf{D}^*,$$

with μ^*_{blood} given by (2.4).

In order to justify (S1), we consider τ, given by (5.19), as new dimensionless time so that the longitudinal convective derivative (6.21) becomes

$$\frac{D}{Dt} = \frac{\partial}{\partial t} + \langle v_x \rangle \frac{\partial}{\partial x} \quad \rightarrow \quad \mathscr{B}_1 \frac{\partial}{\partial \tau} + \langle v_x \rangle \frac{\partial}{\partial x},$$

where $\langle v_x \rangle$ is defined in (6.20). The simplification consists in neglecting $\mathscr{B}_1 \dfrac{\partial \hat{c}_i}{\partial \tau}$, which turns out to be appropriate, since $\mathscr{B}_1 \sim 10^{-3}$. Hence $\dfrac{D}{Dt} \sim \langle v_x \rangle \dfrac{\partial}{\partial x}$.

Equations $(4.1)_9$, $(4.1)_7$ with boundary conditions (5.1) and (5.2) give rise to the following Cauchy problem

$$(6.2) \quad \begin{cases} \langle v_x \rangle \dfrac{\partial \hat{c}_p}{\partial x} = 2 \dfrac{\hat{c}_p}{1 - \phi} \dfrac{\mu \mathsf{S} \mathsf{G}}{\ln H} (P_{ch} - P_s - \mathsf{Os}\, \hat{\Pi}(\hat{c}_p)), & 0 < x < 1, \\[3mm] \langle v_x \rangle \dfrac{\partial \phi}{\partial x} = 2\phi \dfrac{\mu \mathsf{S} \mathsf{G}}{\ln H} (P_{ch} - P_s - \mathsf{Os}\, \hat{\Pi}(\hat{c}_p)), & 0 < x < 1, \\[3mm] \phi|_{x=0} = \phi_o, \quad \hat{c}_p|_{x=0} = 1. \end{cases}$$

Concerning the solutes, equation $(4.1)_{10}$ simplifies to this initial value problem[16]

$$(6.3) \quad \begin{cases} \langle v_x \rangle \dfrac{\partial \hat{c}_i}{\partial x} = -2\hat{c}_i \mathfrak{D}_i \left(1 - \dfrac{\mathrm{r}_i^{(d)}}{\hat{c}_i} \right) & i = \mathrm{U, Na}. \\[3mm] \hat{c}_i(0, \tau) = \hat{c}_{i,in}(\tau), \end{cases}$$

with $\hat{c}_{i,in}(t)$, $i = \mathrm{U, Na}$, given by (5.12). Since neither $\langle v_x \rangle$, nor ϕ, depend on $\hat{c}_i$, we solve (6.3), getting[17]

$$\hat{c}_i(x, \tau) = \underbrace{\hat{c}_{i,in}(\tau)}_{\frac{M_{i,ec}}{V_{ec}}} \exp \left\{ -\int_0^x \frac{2\mathfrak{D}_i}{\langle v_x \rangle} dx' \right\} + \mathrm{r}_i^{(d)} \left(1 - \exp \left\{ -\int_0^x \frac{2\mathfrak{D}_i}{\langle v_x \rangle} dx' \right\} \right).$$

Thus, recalling (5.16) and (5.17) and introducing the parameter

$$(6.4) \quad A = \frac{2\mu \mathsf{G} \mathsf{S}}{\ln H},$$

we rewrite $\mathfrak{J}_i$, $i = \mathrm{U, Na}$, as follows

$$(6.5) \quad \mathfrak{J}_\mathrm{U} = \frac{M_{\mathrm{U},ec}(\tau)}{V_{ec}(\tau)} \mathscr{B}_3,$$

$$(6.6) \quad \mathfrak{J}_\mathrm{Na} = \frac{M_{\mathrm{Na},ec}(\tau)}{V_{ec}(\tau)} \mathscr{B}_4 + \mathrm{r}_\mathrm{Na}^{(d)} \mathscr{B}_5,$$

where

$$(6.7) \quad \mathscr{B}_3 = \frac{16}{3} \frac{\mathscr{B}_2}{\mathscr{B}_1} \int_0^1 \exp \left\{ -\int_0^x \frac{2\mathfrak{D}_\mathrm{U}}{\langle v_x \rangle} dx' \right\}$$
$$\cdot \left[\frac{A}{2} (P_{ch} - P_s - \mathsf{Os}\, \hat{\Pi}(\hat{c}_p)) + (1 - \phi) \mathfrak{D}_\mathrm{U} \right] dx,$$

---

[16] Again we have neglected the partial derivative of $\hat{c}_i$ w.r.t. τ.
[17] The typical values of $\mathrm{r}_i^{(d)}$, $i = \mathrm{U, Na}$, are reported in Table 10.

(6.8)
$$\mathcal{B}_4 = \frac{16}{3} \frac{\mathcal{B}_2}{\mathcal{B}_1} \int_0^1 \exp\left\{ -\int_0^x \frac{2\mathfrak{D}_{\mathrm{Na}}}{\langle v_x \rangle} \, dx' \right\}$$
$$\cdot \left[\frac{A}{2} (P_{ch} - P_s - \mathsf{Os}\,\hat{\Pi}(\hat{c}_p)) + (1 - \phi)\mathfrak{D}_{\mathrm{Na}} \right] dx,$$

and

(6.9)
$$\mathcal{B}_5 = \frac{16}{3} \frac{\mathcal{B}_2}{\mathcal{B}_1} \int_0^1 \left[\frac{A}{2}\left(1 - \exp\left\{ -\int_0^x \frac{2\mathfrak{D}_{\mathrm{Na}}}{\langle v_x \rangle} \, dx' \right\}\right)(P_{ch} - P_s - \mathsf{Os}\,\hat{\Pi}(\hat{c}_p)) \right.$$
$$\left. - (1 - \phi)\mathfrak{D}_{\mathrm{Na}} \exp\left\{ -\int_0^x \frac{2\mathfrak{D}_{\mathrm{Na}}}{\langle v_x \rangle} \, dx' \right\} \right] dx$$

Hence problem (5.20) can be rewritten as follows

(6.10)
$$\begin{cases} \dfrac{d}{d\tau}\left[\dfrac{3}{8} V_{ex} + \dfrac{5}{8} V_{ic} \right] = -\dot{\mathscr{R}}, \\[2ex] \dfrac{dM_{\mathrm{U},ic}}{d\tau} = -\dfrac{8}{5}\left(\dfrac{M_{\mathrm{U},ic}}{V_{ic}} - \dfrac{M_{\mathrm{U},ec}}{V_{ec}} \right), \\[2ex] \dfrac{dM_{\mathrm{U},ec}}{d\tau} = \dfrac{8}{3}\left(\dfrac{M_{\mathrm{U},ic}}{V_{ic}} - \dfrac{M_{\mathrm{U},ec}}{V_{ec}} \right) + \mathscr{G}_{\mathrm{U}} - \mathcal{B}_3 \dfrac{M_{\mathrm{U},ec}(\tau)}{V_{ec}(\tau)}, \\[2ex] \dfrac{dM_{\mathrm{Na},ec}}{d\tau} = \mathscr{G}_{\mathrm{Na}} - \mathcal{B}_4 \dfrac{M_{\mathrm{Na},ec}(\tau)}{V_{ec}(\tau)} - \mathcal{B}_5, \\[2ex] \dfrac{V_{ic}(t)}{V_{ec}(t)}\left[\mathscr{A}_1 M_{\mathrm{Na},ec}(t) + \mathscr{A}_2 M_{\mathrm{U},ec}(t) + \mathscr{A}_3 \right] - \mathscr{A}_2 M_{\mathrm{U},ic}(t) - \dfrac{3}{5} = 0. \end{cases}$$

Concerning the simplifying assumption (S2), namely the rheological model (6.1), we exploit it in $(4.1)_1$, obtaining

$$\frac{\lambda(\hat{c}_p)}{8}\left(1 + \frac{5}{2}\phi\right)\frac{\partial v_x}{\partial r} = -\frac{r}{2}\left(-\frac{\partial P_{ch}}{\partial x} + \mathsf{R}_{\mathsf{p}} g_x \right).$$

Next, we simplify also B.C. $(4.1)_2$, considering $\mathsf{B} \to \infty$ (i.e. a no-slip condition). So, integrating the above equation between r and 1, and then averaging according to (6.20), we obtain

(6.11)
$$\langle v_x \rangle = \frac{\mathsf{R}_{\mathsf{p}} g_x - \dfrac{\partial P_{ch}}{\partial x}}{\lambda(\hat{c}_p)\left(1 + \dfrac{5}{2}\phi\right)},$$

which is the expression to be inserted in (6.2) and in (6.7)–(6.9).

The equation for the pressure field P_{ch} is obtained exploiting $(4.1)_3$, so to get the boundary value problem

$$(6.12) \quad \begin{cases} \dfrac{\partial^2 P_{ch}}{\partial x^2} = A\lambda_1 \left[1 - \dfrac{9\lambda_2}{2\lambda_1}\left(\dfrac{\hat{c}_p \phi}{1-\phi}\right)\right][P_{ch} - (P_s + \mathrm{Os}\,\hat{\Pi}(\hat{c}_p))], \\ P_{ch}(0) = 1, \quad P_{ch}(1) = 0, \end{cases}$$

with λ_1, and λ_2, defined in (2.5) and reported in Table 2.

Thus the dynamics of the dependent variables $\{\phi, \hat{c}_p, P_{ch}, P_s\}$, is governed by the Cauchy problem (6.2) and the boundary values problem (6.12) and $(4.1)_5$, $(4.1)_6$. For the reader's convenience we summarize the whole simplified model

$$(6.13) \quad \begin{cases} \dfrac{\partial \phi}{\partial x} = A\phi \left[\dfrac{\lambda(\hat{c}_p)\left(1 + \dfrac{5}{2}\phi\right)}{\mathsf{R}_p g_x - \dfrac{\partial P_{ch}}{\partial x}}\right][P_{ch} - (P_s + \mathrm{Os}\,\hat{\Pi}(\hat{c}_p))], \\[4mm] \dfrac{\partial \hat{c}_p}{\partial x} = \dfrac{\hat{c}_p}{1-\phi} A \left[\dfrac{\lambda(\hat{c}_p)\left(1 + \dfrac{5}{2}\phi\right)}{\mathsf{R}_p g_x - \dfrac{\partial P_{ch}}{\partial x}}\right][P_{ch} - (P_s + \mathrm{Os}\,\hat{\Pi}(\hat{c}_p))], \\[4mm] \dfrac{\partial^2 P_{ch}}{\partial x^2} = A\lambda_1 \left[1 - \dfrac{9\lambda_2}{2\lambda_1}\left(\dfrac{\hat{c}_p \phi}{1-\phi}\right)\right][P_{ch} - (P_s + \mathrm{Os}\,\hat{\Pi}(\hat{c}_p))], \\[4mm] \dfrac{\partial^2 P_s}{\partial x^2} = \dfrac{\mathsf{G}}{\mathfrak{R}_0}[P_s - P_{ch} + \mathrm{Os}\,\hat{\Pi}(\hat{c}_p)], \\[2mm] \phi|_{x=0} = \phi_o, \quad \hat{c}_p|_{x=0} = 1, \quad P_{ch}(0) = 1, \quad P_{ch}(1) = 0, \\ P_s(0) = P_{s,in}, \quad P_s(1) = P_{s,out}. \end{cases}$$

Once solved, we compute the constants $\mathscr{B}_3$, $\mathscr{B}_4$, and $\mathscr{B}_5$, given by (6.7)–(6.9), as well as $\dot{\mathscr{R}}$, and solve problem (6.10). In particular, we are in position to evaluate the extraction rates. Indeed

$$\dot{\mathscr{R}}^* = K_U^* V_T^*(0)\dot{\mathscr{R}} \underset{\text{Table 8}}{=} 0.77\dot{\mathscr{R}} \text{ lt/min,}$$

$$\mathfrak{J}_U^* = \frac{3}{8}\frac{M_{U,ec}^*(0)}{V_{ec}^*(0)} K_U^* V_T^*(0)\mathfrak{J}_U \underset{\text{Table 8}}{=} 2.9\mathfrak{J}_U \text{ mmol/min}$$

$$\underset{(6.5)}{=} 2.9\frac{M_{U,ec}(\tau)}{V_{ec}(\tau)}\mathscr{B}_3 \text{ mmol/min,}$$

and

$$\mathfrak{J}_{Na}^* = \frac{3}{8}\frac{M_{Na,ec}^*(0)}{V_{ec}^*(0)} K_U^* V_T^*(0)\mathfrak{J}_{Na} \underset{\text{Table 8}}{=} 40.4\mathfrak{J}_{Na} \text{ mEq/min}$$

$$\underset{(6.6)}{=} 40.4\left(\frac{M_{Na,ec}(\tau)}{V_{ec}(\tau)}\mathscr{B}_4 + \mathrm{r}_{Na}^{(d)}\mathscr{B}_5\right) \text{ mEq/min,}$$

The numerical simulations shown in the figures 6–16 below refer to the simplified blood rheological model, with the data specified in the various Tables of the paper.

We start with the total proteins concentration Fig. 6 and the hematocrit Fig. 7. Figure 8 shows the blood pressure profile, while Fig. 9 dialyzate pressure. Actu-
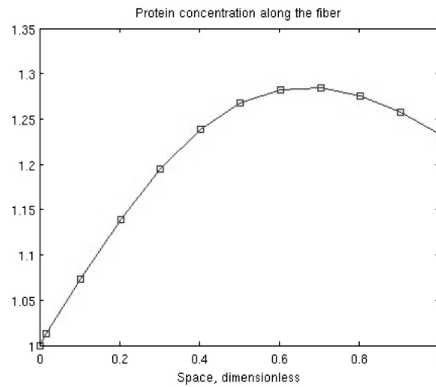

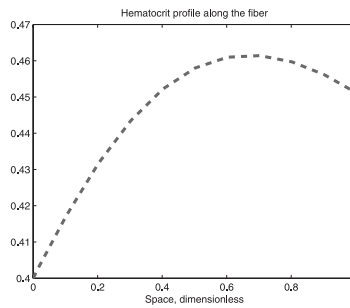Figure 6. Total Proteins concentration profile (dimensionless).
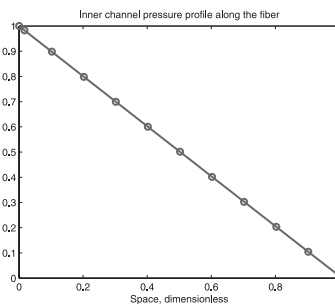

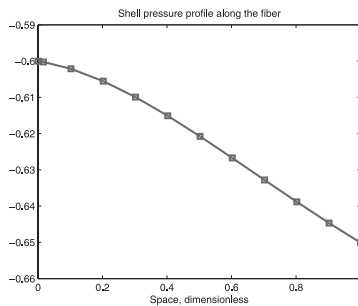Figure 7. Hematocrit profile.

Figure 8. Blood pressure profile (dimensionless) within the fiber.

Figure 9. Dialyzed pressure profile (dimensionless).
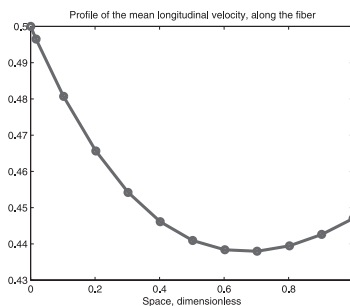
Figure 10. Longitudinal velocity profile (dimensionless).
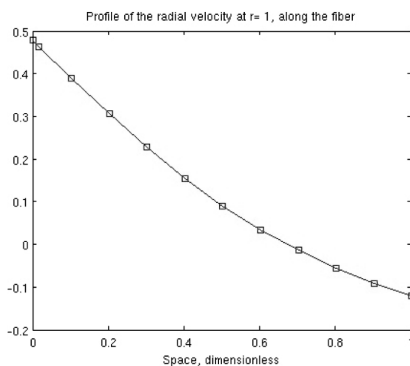
Figure 11. Radial velocity profile (dimensionless).

ally $P_{ch}(x)$ is almost linear, while $P_s(x)$ shows a non-linear behavior close to $x = 0$. We note that $\left| \dfrac{\partial^2 P_{ch}}{\partial x^2} \right| \sim 10^{-2}$, while $\left| \dfrac{\partial^2 P_s}{\partial x^2} \right|$ is an order of magnitude larger (especially close to $x = 0$). This explains the different qualitative aspect of $P_{ch}(x)$ and $P_s(x)$.
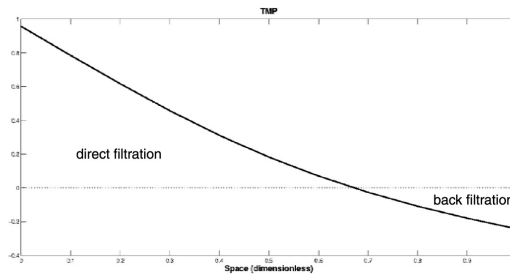
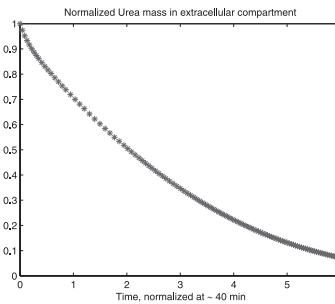Figure 12. Trans-Membrane Pressure (dimensionless).

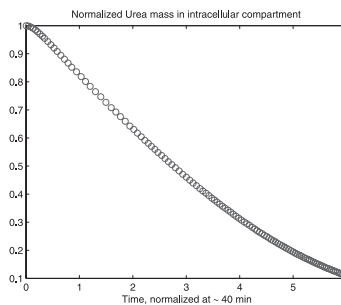Figure 13. Extracellular urea mass (dimensionless).

Figure 14. Intracellular urea mass (dimensionless).

We note that TMP, reported in Fig. 12, is largely amplified in equations $(6.13)_1$ and $(6.13)_2$ by the respective coefficients. We also note that, close to $x \sim 0.7$, TMP becomes negative meaning that backfiltration is active. This fact is also highlighted in Fig. 11. The mean longitudinal velocity (namely the discharge) is plotted, as a function of the longitudinal coordinate, in Fig. 10. Again we note that, after $x \sim 0.7$, $\langle v_x \rangle$ starts growing. This is due to the external liquid sucked back by osmosis. Indeed, the selected data are such that oncotic pressure builds up in such a way that the radial velocity becomes negative for $0.7 \lesssim x \leq 1$,
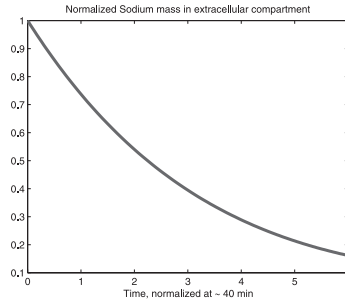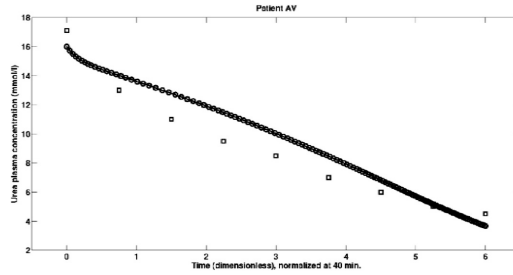
Figure 15. Sodium mass (dimensionless).

Figure 16. Urea concentration in plasma. Comparison between the experimental data of [14], patient A.V., and those predicted by the model, for average data.

producing a decrease both of c_p and of ϕ, and correspondingly an increase of the longitudinal blood velocity.

Extracellular, intracellular urea and extracellular Na^+ masses are plotted as functions of time (see Fig. 13, 14, 15). In Figure 16 we have reported the comparison between the simulation referred to average data and the experimental data for a specific patient, reported in [14].

APPENDIX A. DERIVATION OF SYSTEM (4.1)

The derivation of (4.1) is based on the assumptions listed in section 4.

Flow in the inner channel

Let us write the strain rate tensor $\mathbf{D}^*$

$$\mathbf{D}^* = \frac{v_{ref}^*}{L^*} \begin{pmatrix} \dfrac{\partial v_x}{\partial x} & \dfrac{1}{2\varepsilon}\left(\dfrac{\partial v_x}{\partial r} + \varepsilon^2 \dfrac{\partial v_r}{\partial x}\right) & 0 \\[3mm] \dfrac{1}{2\varepsilon}\left(\dfrac{\partial v_x}{\partial r} + \varepsilon^2 \dfrac{\partial v_r}{\partial x}\right) & \dfrac{\partial v_r}{\partial r} & 0 \\[3mm] 0 & 0 & \dfrac{v_r}{r} \end{pmatrix}.$$

Hence,

$$II_{\mathbf{D}^*}^* = \frac{1}{\varepsilon}\left(\frac{v_{ref}^*}{L^*}\right)\left|\frac{\partial v_x}{\partial r}\right| + \mathcal{O}(1).$$

The continuity equations for RBC's and blood as a whole can be written as

(6.14) $$\frac{\partial \phi}{\partial t^*} + \nabla^* \cdot (\phi \vec{v}_{RBC}^*) = 0, \quad \text{(RBC's)},$$

(6.15) $$\nabla^* \cdot \vec{v}^* = 0, \quad \Leftrightarrow \quad \operatorname{tr}\mathbf{D}^* = 0, \quad \text{(blood incompressibility)}.$$

In particular, the latter acquires the dimensionless form

(6.16) $$\frac{\partial v_x}{\partial x} + \frac{1}{r}\frac{\partial}{\partial r}(rv_r) = 0.$$

Now, recalling the definition (2.2), Assumption 1 entails

(6.17) $$\begin{cases} v_{pl,x}^* = v_{RBC,x}^* = v_x^*, \\ v_{pl,r}^* = \dfrac{1}{1-\phi}v_r^*, \quad \Rightarrow \quad v_r^* = (1-\phi)v_{pl,r}^*, \end{cases}$$

respectively. Then, exploiting again this assumption, (6.14) can be given the dimensionless form

(6.18) $$\frac{\partial \phi}{\partial t} + v_x\frac{\partial \phi}{\partial x} + \phi\frac{\partial v_x}{\partial x} = 0.$$

Taking (6.16) into account, equation (6.18) can be further elaborated, obtaining

(6.19) $$\frac{\partial \phi}{\partial t} + v_x\frac{\partial \phi}{\partial x} = \phi\frac{1}{r}\frac{\partial}{\partial r}(rv_r).$$

Next, we introduce the mean longitudinal blood velocity

(6.20) $$\langle v_x\rangle = 2\int_0^1 rv_x\,dr,$$

and the longitudinal convective derivative (following the blood)

(6.21) $$\frac{D}{Dt} = \frac{\partial}{\partial t} + \langle v_x\rangle\frac{\partial}{\partial x}.$$

We integrate (6.19) in r over the channel lumen (namely, for $0 \le r \le 1$), obtaining by virtue of (6.17)$_2$,

(6.22) $$\frac{1}{\phi}\frac{D\phi}{Dt} = 2v_r|_{r=1} = 2(1-\phi)v_{pl,r}|_{r=1},$$

which has an evident physical meaning: the relative hematocrit change per unit time is proportional to the plasma out-flux (or influx) through the membrane inner wall. In particular, when $v_r|_{r=1}$, ϕ increases (as physically expected) since plasma flows out from the vessel.

Following [38], the motion equation for the blood (i.e. the fluid mixture) as a whole is

$$\rho^*\left(\frac{\partial \vec{v}^*}{\partial t^*} + \vec{v}^* \cdot \nabla^* \vec{v}^*\right) = \rho^* \vec{g}^* + \nabla^* \cdot \mathbf{T}^*,$$

where $\mathbf{T}^*$ is given by (2.3), and $\vec{g}^*$ gravity acceleration. Hence, keeping only the leading terms[18] the dimensionless motion equations for the blood take the form

(6.23) $$\frac{\partial P_{ch}}{\partial x} = \mathsf{R_P} g_x + \frac{1}{8r}\frac{\partial}{\partial r}\left[r\lambda(\hat{c}_p)\left(1 + \frac{5}{2}\phi\gamma\left(\frac{\partial v_x}{\partial r}\right)\right)\frac{\partial v_x}{\partial r}\right],$$

(6.24) $$\frac{\partial P_{ch}}{\partial r} = 0,$$

where $g_x = \frac{\vec{g}^*}{|\vec{g}^*|} \cdot \vec{e}_x$, is the component of the acceleration gravity along the longitudinal axis, and $\mathsf{R_P}$ is given by (4.2). In particular, with the data of Tables 1 and 4, $\mathsf{R_P} \sim 0.5$.

Flow within the porous membrane

The membrane is modeled as a uniform medium whose permeability K^*. In the membrane the flow governing equations are

$$\begin{cases} \nabla^* \cdot \vec{q}^* = 0, & \text{continuity equation,} \\ \vec{q}^* = -\dfrac{K^*}{\mu^*_{H_2O}}\nabla^* p^*_m, & \text{Darcy's law,} \end{cases}$$

Thus, neglecting $\mathcal{O}(\varepsilon^2)$ terms, we get, $\dfrac{\partial}{\partial r}\left(r\dfrac{\partial P_m}{\partial r}\right) = 0$, whose solution is

(6.25) $$P_m = (P_m|_{r=H} - P_m|_{r=1})\frac{\ln r}{\ln H} + P_m|_{r=1}.$$

In particular, writing the radial component of Darcy's law in non-dimensional form, recalling (2.9), (3.5) and (3.15) we obtain

(6.26) $$q_r = -\frac{S}{\Delta P_{TM}}\frac{\partial P_m}{\partial r} = -\frac{S}{\Delta P_{TM}}\frac{(P_m|_{r=H} - P_m|_{r=1})}{\ln H}\frac{1}{r}.$$

We notice that $q_r > 0$ (positive radial flow) when $P_m|_{r=1} > P_m|_{r=H}$.

---

[18] The Reynolds number, $\mathsf{Re} = \dfrac{\rho^* v^*_{ref} R^*}{\mu^*_{ref}}$, is ~ 1.

Dialyzate flow

Mechanical incompressibility (2.8) is expressed by

$$(6.27) \qquad \frac{\partial w_x}{\partial x} + \frac{1}{r}\frac{\partial}{\partial r}(rw_r) = 0,$$

where (3.6) has been exploited. The flow is governed by the Navier–Stokes equation

$$(6.28) \qquad \rho^*\left(\frac{\partial \vec{w}^*}{\partial t^*} + \vec{w}^* \cdot \nabla^* \vec{w}^*\right) = -\nabla^* P_s^* + \rho^* \vec{g}^* + \mu_{H_2O}^* \Delta^* \vec{w}^*.$$

So, neglecting inertia (recall that the Reynolds number is ~ 1) and keeping only the leading terms, the dimensionless form of the above equations is

$$(6.29) \qquad -\frac{\partial P_s}{\partial x} + \mathsf{R_P} g_x + \frac{\mathsf{F}}{r}\frac{\partial}{\partial r}\left(r\frac{\partial w_x}{\partial r}\right) = 0,$$

$$(6.30) \qquad \frac{\partial P_s}{\partial r} = 0,$$

where again g_x is the component of the unit vector $\vec{g}^*/|\vec{g}^*|$, along the x axis and along the radial direction, the constant F is given by (3.21) and $\mathsf{R_P}$ by (4.2).

Dynamics of the solutes

Let us first consider proteins. Recalling (2.6), we set

$$(6.31) \qquad c_p = \frac{c_p^*}{\hat{c}_{p,ref}^*} = (1-\phi)\frac{\hat{c}_p^*}{\hat{c}_{p,ref}^*} \underset{(2.6)}{=} (1-\phi)\hat{c}_p.$$

In Appendix B we show that c_p, evolves according to (6.66). In other words, considering Assumption 2, the evolution equation of $\hat{c}_p$ has the same structure of (6.22), i.e.

$$(6.32) \qquad \frac{1}{(1-\phi)\hat{c}_p}\frac{D[(1-\phi)\hat{c}_p]}{Dt} = 2v_r|_{r=1} = 2(1-\phi)v_{pl,r}|_{r=1}.$$

Considering the light solutes, we define

$$(6.33) \qquad \hat{c}_i = \frac{\hat{c}_i^*}{\hat{c}_{i,ref}^*}, \quad \text{and} \quad c_i = \frac{c_i^*}{\hat{c}_{i,ref}^*} = (1-\phi)\hat{c}_i, \quad i = 1,\ldots,N,$$

where $\hat{c}_{i,ref}^*$ denotes the reference value for the concentration of the ith solute in the plasma (see section 5). Recalling Assumption 3, and referring

to Appendix B for more details, we show that the evolution of $\hat{c}_i$ is governed by[19]

$$(6.34) \qquad \frac{1}{\hat{c}_i} \frac{D\hat{c}_i}{Dt} = -2\mathfrak{D}_i \left(1 - \frac{c_{i,d}^*}{\hat{c}_i \hat{c}_{i,ref}^*}\right),$$

where $c_{i,d}^*$, is the concentration of the ith solute in the dialyzate, and where

$$(6.35) \qquad \mathfrak{D}_i = \frac{L^* \mathfrak{D}_i^*}{v_{ref}^* R^{*2}} = \frac{\mathfrak{D}_i^* t_{ref}^*}{R^{*2}}, \quad i = 1, \ldots, N,$$

accounts for the diffusion of the ith low molecular compound through the membrane[20]. Indeed, $\mathfrak{D}_i^*$, $[\mathfrak{D}_i^*] = cm^2/s$, is the effective diffusivity coefficient, whose typical order of magnitude is[21] 10^{-5} cm^2/s, [1], so that $\mathfrak{D}_i \sim 1$. Introducing then

$$(6.36) \qquad r_i^{(d)} = \frac{c_{i,d}^*}{\hat{c}_{i,ref}^*}, \quad i = 1, 2, \ldots, N,$$

we can write (6.34) as

$$(6.37) \qquad \frac{1}{\hat{c}_i} \frac{D\hat{c}_i}{Dt} = -2\mathfrak{D}_i \left(1 - \frac{r_i^{(d)}}{\hat{c}_i}\right).$$

In Table 10 we have reported the typical values of $\mathfrak{D}_i$, $\hat{c}_{i,ref}^*$, and $r_i^{(d)}$, for urea, $i = U$, and sodium $i = Na$.

	Value	Source of data
$\mathfrak{D}_U = \mathfrak{D}_{Na}$	~ 1	[1], [14]
$\hat{c}_{U,ref}^*$	10 mmol/lt	[14]
$\hat{c}_{Na,ref}^*$	140 mmol/lt	[14]
$r_U^{(d)}$	0	
$r_{Na}^{(d)}$	~ 0.1	[14]

Table 10. Solutes characteristic quantities. $\hat{c}_{Na,ref}^*$, and $\hat{c}_{U,ref}^*$, are defined by formula (5.11).

---

[19] Recalling (2.1) and (6.33) $c_i = (1 - \phi)\hat{c}_i$, $i = 1, \ldots, N$.

[20] We are considering a negligible concentration of the ith compound in the dialyzate. As a consequence, the diffusive flux through the membrane is proportional to c_i.

[21] If $\mathfrak{D}_i^* \sim 10^{-5}$ cm^2/s, the dialyzer clearance, defined as $\mathcal{N}\mathfrak{D}_i^* L^*$, ranges around 0.2 lt/min, in agreement with the values reported in [14].

Boundary conditions

Referring to Fig. 2, first we state the BC's for $r = 1$, $r = H$ and $r = D$, respectively. The channel and shell inlet and outlet BC's are given by (3.9) and (3.10), respectively.

Internal membrane surface $\{0 \leq x \leq 1, r = 1\}$.   The boundary conditions we impose are:

1. Mass conservation for the fluid (see [13] for instance), namely

$$(6.38) \qquad (1 - \phi) v^*_{pl\,r}|_{r^*=R^*} = q^*_r|_{r^*=R^*}.$$

Hence, recalling $(6.17)_2$, we obtain

$$v^*_r|_{r^*=R^*} = q^*_r|_{r^*=R^*},$$

which, in a dimensionless form, can be rewritten as

$$(6.39) \qquad v_r|_{r=1} = (\mu \mathsf{G} \Delta P_{TM}) q_r|_{r=1},$$

with G given by (3.18), μ by (3.17) and ΔP_{TM} by (3.8). In particular, remembering (6.26)

$$(6.40) \qquad v_r|_{r=1} = -\frac{\mu \mathsf{G} S}{\ln H} \left(P_m|_{r=H} - P_m|_{r=1} \right).$$

We remark that $v_r|_{r=1} > 0$, if $P_m|_{r=1} > P_m|_{r=H}$, as physically expected.
2. Saffman's condition [45] for the slip velocity

$$(6.41) \qquad -\frac{\partial v^*_x}{\partial r^*}\bigg|_{r^*=R^*} = \frac{\alpha_{BJ}}{\sqrt{K^*}} v^*_x|_{r^*=R^*},$$

where α_{BJ} is the Beavers–Joseph constant (non-dimensional) relative to the channel porous wall [4]. Though we have borrowed (6.41) from the theory of liquid/porous interfaces (see e.g. [22]), we must point out that in the present case slip is not due to membrane roughness, but to the composite nature of blood[22].
The dimensionless form of (6.41) is

$$(6.42) \qquad \frac{1}{\mathsf{B}} \frac{\partial v_x}{\partial r}\bigg|_{r=1} = -v_x|_{r=1}.$$

---

[22] It is well known that blood flow in not too small vessels is characterized by the presence of a thin plasma layer, in which the no-slip condition may have sense. However, treating blood as a homogeneous fluid, we must somehow translate in the model the fact that the large RBC's component does not stick to the wall. Hence the necessity of allowing some slip.

with

$$(6.43) \qquad \mathsf{B} = \frac{\alpha_{\mathrm{BJ}}}{\sqrt{\mathsf{Da}}}.$$

and Da given by (3.19). At this stage we do not specify the order of magnitude of B. We rather say that, when $\mathsf{B} = \mathscr{O}(1/\varepsilon)$, (6.42) reduces (at the zero order in ε) to a no-slip condition, i.e. $v_x|_{r=1} = 0$, while, when $\mathsf{B} = \mathscr{O}(1)$, (6.42) makes slip come into play (which is actually our case).

3. Pressure jump due to the oncotic pressure Π^*, given by (2.10). We have

$$p_{ch}^*|_{r^*=R^*} = p_m^*|_{r^*=R^*} + \Pi^*.$$

Dividing both members by ΔP_{ch}^*, and recalling (3.13), we get

$$(6.44) \qquad P_m|_{r=1} = P_{ch}|_{r=1} - \mathsf{Os}\,\hat{\Pi}(\hat{c}_p),$$

where the function $\hat{\Pi}(\hat{c}_p)$ is defined by (3.12), and Os by (3.13).

External membrane surface $\{0 \leq x \leq 1, r = H\}$. The boundary condition we impose are similar to the ones previously stated, namely:

1. Mass conservation, that is

$$w_r^*|_{r^*=H^*} = q_r^*|_{r^*=H^*}.$$

Recalling (3.16) and (3.20), we have

$$w_r|_{r=H} = \frac{\mathsf{G}\Delta P_{TM}}{\mathsf{F}}\,q_r|_{r=H},$$

or, by virtue of (6.26),

$$(6.45) \qquad w_r|_{r=H} = -\frac{\mathsf{G}S}{\mathsf{F}}\frac{(P_m|_{r=H} - P_m|_{r=1})}{H \ln H},$$

with G given by (3.18) and F by (3.21).

2. No slip condition

$$(6.46) \qquad w_x|_{r=H} = 0.$$

3. Pressure continuity,

$$(6.47) \qquad P_s|_{r=H} = P_m|_{r=H}.$$

On $r = H$, there are no osmosis effect.

External "virtual" surface $\{0 \leq x \leq 1, r = D\}$. We impose impermeability and symmetry

$$(6.48) \qquad w_r|_{r=D} = 0, \quad \text{and} \quad \left.\frac{\partial w_x}{\partial r}\right|_{r=D} = 0.$$

Symmetry axis $\{0 \leq x \leq 1, r = 0\}$.

$$(6.49) \qquad \left.\frac{\partial v_x}{\partial r}\right|_{r=0} = 0.$$

Inlet values $\{x = 0, 0 \leq r \leq 1\}$. The model needs inlet conditions for hematocrit and solutes concentration, which, at this stage, are not available. So, as first instance, we set

$$\phi|_{x=0} = \phi_{in}(t), \quad \hat{c}_p|_{x=0} = \hat{c}_{p,in}(t), \quad \hat{c}_i|_{x=0} = \hat{c}_{i,in}(t), \quad i = 1, 2, \ldots, N.$$

Actually, as pointed out in [17], the issue of the inlet values is by no means trivial. It will be discussed in section 5.

Initial conditions. We set

$$(6.50) \qquad \phi(x, 0) = \phi_o,$$

and

$$(6.51) \qquad \hat{c}_p^*(x^*, 0) = \hat{c}_{po}^*, \quad \text{and} \quad \hat{c}_i^*(x^*, 0) = \hat{c}_{io}^*, \quad i = 1, \ldots N.$$

all values being taken before the treatment.

Model upscaling

The neat separation of scales enables us to apply an upscaling procedure, expanding all relevant quantities in powers of epsilon and matching terms of similar order in the governing equations. We proceed to the derivation of the governing equations at the ε^0 order approximation.

Outer shell. From (6.30), we derive $P_s = P_s(x, t)$. Hence, integrating (6.29) between r and D, we obtain

$$(6.52) \qquad \frac{\partial w_x}{\partial r} = \frac{1}{2\mathsf{F}} \left(-\frac{\partial P_s}{\partial x} + \mathsf{R_P} g_x \right) \left(\frac{D^2}{r} - r \right),$$

where boundary condition (6.48) has been exploited. Next, we integrate (6.52) with the boundary condition (6.46) getting to

$$(6.53) \qquad w_x = \frac{1}{2\mathsf{F}} \left(-\frac{\partial P_s}{\partial x} + \mathsf{R_P} g_x \right) \left\{ D^2 \ln\left(\frac{r}{H}\right) - \frac{1}{2}(r^2 - H^2) \right\}.$$

Now we insert (6.53) into (6.27) and integrate the corresponding in r between H and D. Taking into account $(6.48)_1$ and (6.45)

$$\frac{\mathfrak{K}_0}{\mathsf{G}} \frac{\partial^2 P_s}{\partial x^2} = P_m|_{r=H} - P_m|_{r=1},$$

where

(6.54)
$$\mathfrak{K}_0 = \frac{\ln H}{2S} \int_H^D \left\{ D^2 \ln\left(\frac{r}{H}\right) - \frac{1}{2}(r^2 - H^2) \right\} r\, dr$$

$$= \frac{\ln H}{2S} \left\{ \frac{D^4}{2} \ln\left(\frac{D}{H}\right) - \frac{D^4}{8}\left(3 - \frac{H^2}{D^2}\right)\left(1 - \frac{H^2}{D^2}\right) \right\}.$$

We notice that $\mathfrak{K}_0$, depends only on geometric parameters. In particular, considering the data of Table 1, we have $\mathfrak{K}_0 = 0.486$.

Next, we recall (6.47) and (6.44), so that the pressure field within the shell is obtained solving the following boundary value problem

(6.55)
$$\begin{cases} \dfrac{\partial^2 P_s}{\partial x^2} = \dfrac{\mathsf{G}}{\mathfrak{K}_0} [P_s - P_{ch}|_{r=1} + \mathsf{Os}\, \hat{\Pi}(\hat{c}_p)], \\ P_s(x = 0) = P_{s,in}, \\ P_s(x = 1) = P_{s,out}. \end{cases}$$

with the function $\hat{\Pi}(\hat{c}_p)$, defined by (3.12). It is useful to remark that the r.h.s. $(6.55)_1$ is proportional to G, given by (3.18), hence to the membrane permeability.

Inner channel. Equation (6.24) entails $P_h = P_h(x, t)$. Hence, from (6.23) and (6.42) we obtain the Cauchy problem

(6.56)
$$\begin{cases} \dfrac{\lambda(\hat{c}_p)}{8}\left(1 + \dfrac{5}{2}\phi\gamma\left(\dfrac{\partial v_x}{\partial r}\right)\right)\dfrac{\partial v_x}{\partial r} = -\dfrac{r}{2}\left(-\dfrac{\partial P_{ch}}{\partial x} + \mathsf{R}_p g_x\right), \\ v_x|_{r=1} = -\dfrac{1}{\mathsf{B}}\dfrac{\partial v_x}{\partial r}\bigg|_{r=1}. \end{cases}$$

In particular, $(6.56)_2$ can be also rewritten as

(6.57)
$$\left[\frac{\lambda(\hat{c}_p)}{8}\left(1 + \frac{5}{2}\phi\gamma\left(\frac{\partial v_x}{\partial r}\right)\right)v_x\right]_{r=1} = \frac{1}{2\mathsf{B}}\left(-\frac{\partial P_h}{\partial x} + \mathsf{R}_p g_x\right).$$

Next, we focus on the continuity equation (6.16), which, integrated over a cross section, taking into account (6.49) and (6.40), yields

$$\int_0^1 r\frac{\partial v_x}{\partial x}\, dr = \frac{\mu \mathsf{G} S}{\ln H}(P_m|_{r=H} - P_m|_{r=1}).$$

Recalling then (6.47) and (6.44) we have

$$(6.58) \qquad \int_0^1 r \frac{\partial v_x}{\partial x} dr = \frac{\mu \mathsf{SG}}{\ln H} (P_s - P_{ch} + \mathsf{Os}\,\hat{\Pi}(\hat{c}_p)).$$

We thus obtain the following coupled system

$$(6.59) \qquad \begin{cases} \dfrac{\lambda(\hat{c}_p)}{8} \left(1 + \dfrac{5}{2}\phi\gamma\left(\dfrac{\partial v_x}{\partial r}\right)\right) \dfrac{\partial v_x}{\partial r} = -\dfrac{r}{2}\left(-\dfrac{\partial P_{ch}}{\partial x} + \mathsf{R_p}g_x\right), \\[2mm] v_x|_{r=1} = -\dfrac{1}{\mathsf{B}} \dfrac{\partial v_x}{\partial r}\bigg|_{r=1}, \\[2mm] \displaystyle\int_0^1 r \dfrac{\partial v_x}{\partial x} dr = \dfrac{\mu \mathsf{SG}}{\ln H}(P_s - P_{ch} + \mathsf{Os}\,\hat{\Pi}(\hat{c}_p)), \\[2mm] P_{ch}|_{x=0} = 1, \quad P_{ch}|_{x=1} = 0, \end{cases}$$

where $(6.59)_2$ can be replaced by (6.57).

We now consider equation (6.22) and recall (6.40),

$$\frac{1}{\phi} \frac{D\phi}{Dt} = 2v_r|_{r=1} = 2\frac{\mu \mathsf{SG}}{\ln H}(P_m|_{r=1} - P_m|_{r=H}),$$

which, exploiting (6.44) and (6.47), can be rewritten as

$$(6.60) \qquad \frac{1}{\phi} \frac{D\phi}{Dt} = 2\frac{\mu \mathsf{SG}}{\ln H}(P_{ch} - P_s - \mathsf{Os}\,\hat{\Pi}(\hat{c}_p)),$$

since

$$(6.61) \qquad v_r|_{r=1} = \frac{\mu \mathsf{SG}}{\ln H}(P_{ch} - P_s - \mathsf{Os}\,\hat{\Pi}(\hat{c}_p)).$$

Equation (6.60) emphasizes the progressive increase of ϕ, provided that $P_{ch} > P_s + \mathsf{Os}\,\hat{\Pi}(\hat{c}_p)$.

Concerning $\hat{c}_p$, we proceed in an analogous way so that, recalling (6.31) and (6.60), equation (6.32) acquires the form

$$(6.62) \qquad \frac{1}{\hat{c}_p} \frac{D\hat{c}_p}{Dt} = \frac{2}{1-\phi} \frac{\mu \mathsf{SG}}{\ln H}(P_{ch} - P_s - \mathsf{Os}\,\hat{\Pi}(\hat{c}_p)).$$

Thus the complete model is summarized by system (4.1).

APPENDIX B

According to classical mixture theory [38], the continuity equation for the βth, $\beta = p, 1, \ldots, N$, solute can be rewritten as

$$(6.63) \qquad \frac{\partial c_\beta^*}{\partial t^*} + \frac{\partial (J_{\beta,x}^*)}{\partial x^*} + \frac{1}{r^*} \frac{\partial (r^* J_{\beta,r}^*)}{\partial r^*} = 0,$$

where $J^*_{\beta,x}$, and $J^*_{\beta,r}$, are the longitudinal and radial fluxes, respectively. Assuming then $c^*_\beta = c^*_\beta(x^*, t^*)$, $\beta = p, 1, \dots, N$, we multiply (6.63) by $2r^*/R^{*2}$, and integrate over the cross section getting

$$(6.64) \qquad \frac{\partial c^*_\beta}{\partial t^*} + \frac{2}{R^{*2}} \int_0^{R^*} \frac{\partial(J^*_{\beta,x})}{\partial x^*} r^* \, dr^* = -\frac{2}{R^{*2}} \int_0^{R^*} \frac{\partial(r^* J^*_{\beta,r})}{\partial r^*} dr^*.$$

Now we model the l.h.s. of (6.64) as an effective out-flux caused, in general, by two phenomena: convection and diffusion. Hence we stipulate that:

- $J^*_{\beta,x} = c^*_\beta v^*_x$.
- $J^*_{\beta,r}|_{r^*=R^*} = \mathscr{I}^*_{\beta,conv} + \mathscr{I}^*_{\beta,diff}$, $[\mathscr{I}^*_{\beta,conv}] = [\mathscr{I}^*_{\beta,diff}] = gr/cm^2s$, are the effective diffusive and convective fluxes of the βth solute through the membrane.

Hence, c^*_β, $\beta = p, 1, \dots, N$, evolves according to

$$(6.65) \qquad \frac{\partial c^*_\beta}{\partial t^*} + \frac{2}{R^{*2}} \int_0^{R^*} \frac{\partial(c^*_\beta v^*_x)}{\partial x^*} r^* \, dr^* = -\frac{2}{R^*} (\mathscr{I}^*_{\beta,conv} + \mathscr{I}^*_{\beta,diff}),$$

When $\beta = p$, i.e. when we consider the proteins, we have $\mathscr{I}^*_{p,conv} = \mathscr{I}^*_{p,diff} = 0$ (the membrane is not permeable to the proteins). Hence (6.65) reduces to

$$\frac{\partial c^*_p}{\partial t^*} + \frac{\partial c^*_p}{\partial x^*} \left(\frac{2}{R^{*2}} \int_0^{R^*} v^*_x r^* \, dr^* \right) + \frac{2c^*_p}{R^{*2}} \left(\int_0^{R^*} \frac{\partial v^*_x}{\partial x^*} r^* \, dr^* \right) = 0.$$

Considering then the dimensionless variable (i.e. definition (6.31)) and recalling definition (6.20) along with (6.16), we obtain

$$\frac{1}{c_p} \underbrace{\left(\frac{\partial c_p}{\partial t} + \langle v_x \rangle \frac{\partial c_p}{\partial x} \right)}_{\frac{Dc_p}{Dt}} = 2v_r|_{r=1},$$

i.e.

$$(6.66) \qquad \frac{1}{c_p} \frac{Dc_p}{Dt} = 2v_r|_{r=1} = 2(1 - \phi)v_{pl,r}|_{r=1}.$$

If $\beta = i$, with $i = 1, \dots, N$, (solutes flowing through the membrane) we write (see, e.g., [38])

$$(6.67) \qquad \mathscr{I}^*_{i,conv} = c^*_i v^*_{pl,r}|_{r^*=R^*}, \quad \text{and} \quad \mathscr{I}^*_{i,diff} = \frac{\mathfrak{D}^*_i c^*_i}{R^*} \left(1 - \frac{c^*_{i,d}}{\hat{c}^*_i} \right),$$

where $c^*_{i,d}$ is the concentration of the ith solute in the dialysate and $\mathfrak{D}^*_i$ the is the membrane effective diffusivity, $[\mathfrak{D}^*_i] = cm^2/s$, relative to the ith solute. Then equation (6.65) acquires the form

$$\frac{\partial c_i^*}{\partial t^*} + \frac{\partial c_i^*}{\partial x^*}\left(\frac{2}{R^{*2}}\int_0^{R^*} v_x^* r^* \, dr^*\right)$$

$$= \frac{2c_i^*}{R^*}\underbrace{[v_r^* - v_{pl,r}^*]_{r^*=R^*}}_{-\frac{\phi}{1-\phi}v_r^*\ (6.17)} - \frac{2\mathfrak{D}_i^* c_i^*}{R^{*2}}\left(1 - \frac{c_{i,d}^*}{\hat{c}_i^*}\right).$$

Considering the dimensionless variables and (6.35), for any $i = 1, \ldots, N$, we obtain

$$\frac{1}{c_i}\underbrace{\left(\frac{\partial c_i}{\partial t} + \langle v_x \rangle \frac{\partial c_i}{\partial x}\right)}_{\frac{Dc_i}{Dt}} = -2\left[\frac{\phi}{1-\phi}v_r|_{r=1} + \mathfrak{D}_i\left(1 - \frac{\mathrm{r}_i^{(d)}}{\hat{c}_i}\right)\right],$$

with $\mathrm{r}_i^{(d)}$ given by (6.36). Recalling then (6.33) and (6.22) we have

$$\frac{1}{\hat{c}_i}\frac{D\hat{c}_i}{Dt} = -2\mathfrak{D}_i\left(1 - \frac{\mathrm{r}_i^{(d)}}{\hat{c}_i}\right),$$

that is (6.34). So, the concentration in plasma of the βth solute decreases only because of solute diffusion through the membrane. The considerations presented here generalize the classical Kedem–Katchalsky's model [25]. A limitation of the model consists in the fact that we have neglected the evolution of the concentrations in the dialyzate (suppoing that the supply of fresh dialyzate is fast enough). We plan to extend the model to include the dynamics of such quantities in a future paper.

REFERENCES

[1] H. E. ABACI - S. A. ALTINKAYA, *Modeling of hemodialysis operation*, Annals of Biomedical Engineering, 38, 3347–3362, 2010.

[2] K. ANNAN, *Mathematical modelling for hollow fiber dialyser: blood and HCO_3^--dialysate flow characteristics*, Int. J. Pure Appl. Math., 79, 425–452, 2012.

[3] N. A. BAZAEV - V. M. GRINVALD - S. V. SELISHCHEV, *A Mathematical model for a biotechnological hemodialysis system*, Biomedical Engineering, 44, 79–84, 2010.

[4] G. S. BEAVERS - D. D. JOSEPH, *Boundary conditions at a naturally permeable wall*, J. Fluid Mech., 30, 197–207, 1967.

[5] I. BORSI - A. FARINA - A. FASANO, *Incompressible laminar flow through hollow fibers: a general study by means of a two-scale approach*, ZAMP, 62, 681–706, 2011.

[6] I. BORSI - A. FARINA - A. FASANO - K. R. RAJAGOPAL, *Modelling the combined chemical and mechanical action for blood clotting*, Adv. Math. Analysis Appl., 29, 53–72, 2008.

[7] R. M. BOWEN, *Theory of mixtures*, in Continuum Physics, Vol. 3, Eringen, A. C., ed., Academic Press, New York, 1976.

[8] W. J. BRUINING, *A general description of flows and pressures in hollow fiber membrane modules*, Chem. Eng. Sci., 44, 1441–1447, 1989.

[9] N. M. Brown - F. C. Lai, *Measurement of permeability and slip coefficient of porous tubes*, ASME J. Fluids Eng., 128, 987–992, 2006.

[10] R. Davis - D. T. Leighton, *Shear-induced transport of a particle layer along a porous wall*, Chem. Eng. Sci., 42, 275–281, 1987.

[11] F. Carapau - A. Sequeira, *1D Models for Blood Flow in Small Vessels Using the Cosserat Theory*, Trans. on Mathematics, 5, 54–62, 2006.

[12] J. Cho - I. S. Kim - J. Moon - B. Kwon, *Determining Brownian and shear-induced diffusivity of nano- and micro-particles for sustainable membrane filtration*, in Integrated Concencts in Water Recycling, Khan S. J., Schäfer A. I., Muston M. H., eds., 2005.

[13] J. Coirer, *Mécanique des Milieux Continus*, Dunod, 1997.

[14] L. Colì - M. Ursino - V. Dalmastri - F. Volpe - G. La Manna - G. Avanzolini - S. Stefoni - V. Bonomini, *A simple mathematical model applied to selection of the sodium profile during profiled haemodialysis*, Nephrol Dial Transplant 13, 404–416, 1998.

[15] S. Eloot - D. De Wachter - I. Van Trich - P. Verdonck, *Computational flow in hollow-fiber dialyzers*, Artificial Organs, 26, 590–599, 2002.

[16] R. Fåhraeus - T. Lindqvist, *The viscosity of blood in narrow capillary tubes*, A, J. Physiol., 96, 362–368, 1931.

[17] A. Fasano - A. Farina, *Modeling high flux hollow fibers dialyzers*, Discrte and Continuous Dynamical Sistems, Series B, 17, 1903–1937, 2012.

[18] A. Fasano - R. Santos - A. Sequeira, *Blood coagulation: a puzzle for biologists, a maze for mathematicians*, in Modelling Physiological Flows, Ambrosi D., Quarteroni A., Rozza G., Eds., Springer Italia, to appear.

[19] M. Galach - A. Werynski, *Mathematical modeling of renal replacement therapies*, Biocybernetics Biomed. Eng., 24, 3–18, 2004.

[20] A. C. Guyton, *Textbook of Medical Physiology*, Philadelphia, Saunders, 1986.

[21] J. Himmelfarb - T. A. Ikizler, *Hemodialysis*, N. Engl. J. Med., 363, 1833–1845, 2010.

[22] W. Jäger - A. Mikelić, *Modeling effective interface laws for transport phenomena between an unconfined fluid and a porous medium using homogenization*, Transp. Porous Med., 78, 489–508, 2009.

[23] J. Janela - A. Moura - A. Sequeira, *A 3D non-Newtonian fluid-structure interaction model for blood flow in arteries*, Journal of Computational and Applied Mathematics, 234, 2783–2791, 2010.

[24] A. Kargol, *A mechanistic model of transport processes in porous membranes generated by osmotic and hydrostatic pressure*, J. Membr. Sci., 191, 61–9, 2001.

[25] O. Kedem - A. Katchalsky, *Thermodynamics analysis of the permeability of biological membranes to non-electrolytes*, Biochim. Biophys. Acta, 27, 229–246, 1958.

[26] J. Keener - J. Sneyd, *Mathematical Physiology. II*, System Physiology. Interdisciplinary Applied Mathematics, Vol. 8/II, 2nd Edition, Springer, 2009.

[27] Ki Moo Lim - Eun Bo Shim, *Research Computational assessment of the effects of a pulsatile pump on toxin removal in blood purification*, BioMedical Engineering OnLine, 9, 1–16, 2010.

[28] J. C. Kim - D. Cruz - F. Garzotto - M. Kaushik - C. Teixeria - M. Baldwin - I. Baldwin - F. Nalesso - J. H. Kim - E. Kang - H. C. Kim - C. Ronco, *Effects of dialysate flow configurations in continuous renal replacement therapy on solute removal*, Computational modeling. Blood Purif., 35, 106–111, 2013.

[29] J. C. KIM - J. H. KIM - H. C. KIM - K. G. KIM - J. C. LEE - E. KANG - H. C. KIM - B. G. MIN - C. RONCO, *Three-dimensional dialysate flow analysis in a hollow-fiber dialyzer by perfusion computed tomography*, Int. J. Artificial Organs, 31, 553–560, 2008.

[30] E. M. LANDIS - J. R. PAPPENHEIMER, *Exchange of substances through the capillary walls*, in Handbook of Physiology. Circulation, W. F. Hamilton, Ed., Am. Physiol. Soc., Washington, DC, (1963).

[31] J. K. LEYPOLDT, *Solute fluxes in different treatment modalities*, Nephrology, Dialysis and Transplantation, 15, 3–9, 2000.

[32] E. N. LIGHTFOOT, *Transport phenomena and living systems*, Wiley, New York, 1974.

[33] M. MASSOUDI - J. F. ANTAKI, *An anisotropic constitutive equation for the stress tensor of blood based on mixture theory*, Math. Problems Engineering, doi:10.1155/2008/579172, 2008.

[34] T. L. PALLONE - J. PETERSEN, *A mathematical model of continuous arteriovenus helofiltration predicts performances*, ASAIO Trans, 33, 304–308, 1987.

[35] G. PONTRELLI, *Blood flow through a circular pipe with an impulsive pressure gradient*, M3AS, 10, 187–202, 2000.

[36] A. QUARTERONI - L. FORMAGGIA - A. VENEZIANI, Eds., *Complex Systems in Biomedicine*, Springer, 2006.

[37] D. QUEMADA, *General features of blood circulation in narrow vessels*, in Rodkiewicz C. M., ed. Arteries and Arterial Blood, New York, Springer-Verlag, 1983.

[38] K. R. RAJAGOPAL - L. TAO, *Mechanics of mixtures*, World Scientific, Singapore, 1995.

[39] N. P. REDDY, *Design of Artificial Kidneys*, in Biomedical Engineering and Design Handbook, Volume 2: Applications, (2nd Edition), Kutz M. Ed., Mc Graw Hill, New York, 2009.

[40] C. RONCO - A. BRENDOLAN - M. FERIANI - M. MILAN - P. CONZ - A. LUPI - P. BERTO - M. BETTINI - G. LA GRECA, *A new scintigraphic method to characterize ultrafiltration in hollow fiber dialyzers*, Kidney International, 41, 1383–1393, 1992.

[41] C. RONCO - A. BRENDOLAN - C. CREPALDI - M. RODIGHIERO - M. SCABARDI, *Blood and dialysate flow distributions in hollow-fiber hemodialyzers analyzed by computerized helical scanning technique*, J Am. Soc. Nephrol., 13, 53–61, 2002.

[42] C. RONCO - N. LEVIN - A. BRENDOLAN - F. NALESSO - D. CRUZ - C. OCAMPO - D. KUANG - M. BONELLO - M. DE CAL - V. CORRADI - Z. RICCI, *Flow distribution analysis by helical scanning in polysulfone hemodialyzers: Effects of fiber structure and design on flow patterns and solute clearances*, Hemodialysis International, 10, 380–388, 2006.

[43] B. D. ROSE, *Clinical Physiology of Acid-Base and Electrolyte Disorders*, New York, McGraw Hill, 1989.

[44] Y. SANO - A. NAKAYAMA, *A Porous media approach for analyzing a countercurrent dialyzer system*, Journal of Heat Transfer, 134, 072602-1–072602-11, 2012.

[45] P. SAFFMAN, *On the boundary condition at a surface of a porous medium*, Stud. Appl. Matgh. 50, 93–101, 1971.

[46] R. SINGH - R. L. LAURENCE, *Influence of slip velocity at a membrane surface on ultrafiltration performance-II (Tube flow system)*, Int. J. Heat Mass Transfer 12, 731–737, 1979.

[47] K. SMITH - A. SEQUEIRA, *Micro-macro simulations of a shear-thinning viscoelastic kinetic model: applications to blood flow*, Applicable Analysis, doi:10.180/00036811.2010.483765, 2010.

[48] E. M. STARLING, *On the absorption of fluids from the convective tissue spaces*, J. Physiol. 19, 312–319, 1896.

[49] Y. SUZUKI - F. KOHORI - K. SAKAI, *Computer-aided design of hollow fiber dialyzers*, J. Artif. Organs 4, 326–330, 2001.

[50] G. J. TANGELDER - D. W. SLAAF - T. ARTS - R. S. RENEMAN, *Wall shear rates in arterioles in vivo: least estimates for platelets velocity profiles*, Am. J. Physiology, 254, 1059–1064, 1988.

[51] N. TOMISAWA - A. C. YAMASHITA, *Amount of adsorbed albumin loss by dialysis membranes with protein adsorption*, J. Artif. Organs 12, 194–199, 2009.

[52] K. K. YELESWARAPU, *Evaluation of continuum models for characterizing the constitutive behavior of blood*, Ph.D dissertation, University of Pittsburgh, Pittsburgh, Pa, USA, 1996.

[53] M. URSINO - L. COLÌ - G. LA MANNA - M. GRILLI CICILIONI - V. DALMASTRI - A. GIUDICISSI - P. MASOTTI - G. AVANZOLINI - S. STEFONI - V. BONOMINI, *A simple mathematical model of intradialytic sodium kinetics: ''in vivo'' validation during hemodialysis with constant or variable sodium*, Int. J. Art. Organs, 19, 393–403, 1996.

[54] M. URSINO - L. COLÌ - C. BRIGHENTI - L. CHIARI - A. DE PASACLIS - G. AVANZOLINI, *Prediction of solute kinetics, acid-base status, and blood volume changes during profiled hemodialysis*, Annals of Biomedical Engineering, 28, 204–216, 2000.

[55] D. WEIPING - H. LIQUN - Z. GANG - Z. HAIFENG - S. ZHIQUAN - G. DAYONG, *Double porous media model for mass transfer in hemodialyzers*, Int. J. Heat Mass Transfer, 47, 4849–4855, 2004.

[56] A. WÜPPER - F. DELLANNA - C. A. BALDAMUS - D. WOERMANN, *Local transport processes in high-flux hollow fiber dialyzers*, J. Membr. Sci., 131, 81–93, 1997.

[57] M. ZIÓLSTROKEKO - J. A. PIETRZYK - J. GRABSKA-CHRZKASTOWSKA, *Accuracy of hemodialysis modeling*, Kidney International, 57, 1152–1163, 2000.

Claudio Ronco
Department of Nephrology
Ospedale San Bortolo
Vicenza, Italy

Francesco Garzotto
Department of Nephrology
Ospedale San Bortolo
Vicenza, Italy

Jeong Chul Kim
Department of Nephrology
Ospedale San Bortolo
Vicenza, Italy
and
International Renal Research Institute Vicenza (IRRIV)
Vicenza, Italy
and

Institute of Medical and Biological Engineering
Medical Research Center
Seoul National University
Seoul, South Korea

Antonio Fasano
FIAB SpA
Firenze, Italy
and
Dipartimento di Matematica e Informatica ''U. Dini''
Università degli Studi di Firenze
Firenze, Italy
and
IASI-CNR
Roma, Italy
fasano@math.unifi.it

Iacopo Borsi
TEA Sistemi SpA
Pisa, Italy

Angiolo Farina
Dipartimento di Matematica e Informatica ''U. Dini''
Università degli Studi di Firenze
Firenze, Italy
angiolo.farina@uni.it